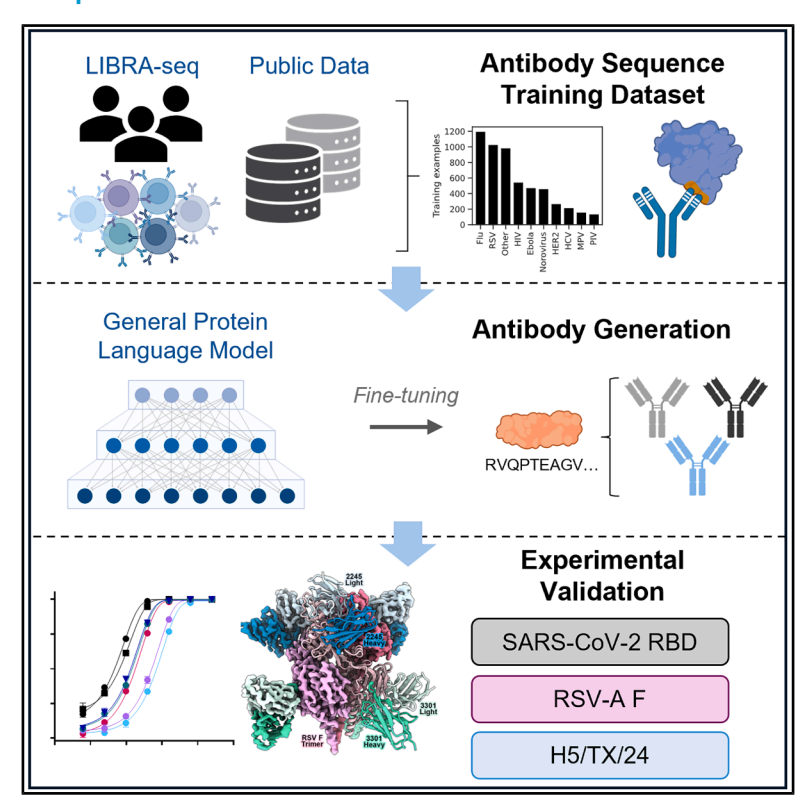


Generation of antigen-specific paired-chain antibodies using large language models

Graphical abstract



Authors

Perry T. Wasdin, Nicole V. Johnson, Alexis K. Janke, ..., Jason S. McLellan, Alexandra A. Abu-Shmais, Ivelin S. Georgiev

Correspondence

ivelin.georgiev@vumc.org

In brief

MAGE is a sequence-based protein language model designed to generate diverse human antibody sequences targeting various pathogens, including SARS-CoV-2, H5N1, and RSV-A. This Aldriven approach addresses traditional limitations by enabling efficient, targetagnostic antibody design with experimentally validated binding specificity.

Highlights

- A protein language model was fine-tuned for antigenspecific antibody generation
- Antibody-antigen sequence database was constructed using public databases and LIBRA-seq
- Antibody design was experimentally validated against RSV-A, SARS-CoV-2, and H5N1
- Generated antibodies showed diverse binding specificities, neutralization, and epitopes







Article

Generation of antigen-specific paired-chain antibodies using large language models

Perry T. Wasdin, ^{1,2,3} Nicole V. Johnson, ⁴ Alexis K. Janke, ^{3,5} Sofia Held, ⁶ Toma M. Marinov, ^{2,3} Gwen Jordaan, ^{3,5} Rebecca A. Gillespie, ⁷ Léna Vandenabeele, ⁶ Fani Pantouli, ⁸ Olivia C. Powers, ^{3,5} Matthew J. Vukovich, ^{3,5} Clinton M. Holt, ^{1,2,3} Jeongryeol Kim, ⁴ Grant Hansman, ⁹ Jennifer Logue, ¹⁰ Helen Y. Chu, ¹⁰ Sarah F. Andrews, ⁷ Masaru Kanekiyo, ⁷ Giuseppe A. Sautto, ⁸ Ted M. Ross, ⁸ Daniel J. Sheward, ⁶ Jason S. McLellan, ⁴ Alexandra A. Abu-Shmais, ^{3,5} and Ivelin S. Georgiev^{1,2,3,5,11,12,13,14,15,16,17,*}

SUMMARY

The traditional process of antibody discovery is limited by inefficiency, high costs, and low success rates. Recent approaches employing artificial intelligence (AI) have been developed to optimize existing antibodies and generate antibody sequences in a target-agnostic manner. In this work, we present MAGE (monoclonal antibody generator), a sequence-based protein language model (PLM) fine-tuned for the task of generating paired human variable heavy- and light-chain antibody sequences against targets of interest. We show that MAGE can generate novel and diverse antibody sequences with experimentally validated binding specificity against SARS-CoV-2, an emerging avian influenza H5N1, and respiratory syncytial virus A (RSV-A). MAGE represents a first-in-class model capable of designing human antibodies against multiple targets with no starting template.

INTRODUCTION

Human monoclonal antibodies are a diverse class of therapeutics that can theoretically target any protein with exquisite specificity, making them promising candidates for treating a wide variety of diseases. Until recently, antibody development has been primarily driven by discovery-based experimental methods, typically through screening human or animal samples with prior exposure to an antigen target of interest. Even with recent developments that have drastically improved the throughput of antibody discovery methods, this process is laborious, slow, and cost-ineffective. The continued growth of the therapeutic market and range of applications for monoclonal antibodies presents an

increased demand for *in silico* tools that accelerate and expand the capabilities of antibody discovery.

Recent breakthroughs in artificial intelligence (AI), most notably the unmatched performance of transformer-based large language models (LLMs) and diffusion models on various tasks, have enabled a surge in computational approaches for antibody-related design tasks. Such methods include affinity maturation, ^{1,2} antibody redesign, ^{1,3,4} and generation of single-domain antibodies. ^{5,6} However, no published methods have demonstrated the ability to design template-free, antigen-specific antibodies. Existing approaches are limited to antibody redesign, with a focus on generation of complementarity-determining regions (CDRs), requiring an initial antibody template to

¹Program in Chemical and Physical Biology, Vanderbilt University Medical Center, Nashville, TN 37232, USA

²Center for Computational Microbiology and Immunology, Vanderbilt University Medical Center, Nashville, TN 37232, USA

³Vanderbilt Center for Antibody Therapeutics, Vanderbilt University Medical Center, Nashville, TN 37232, USA

⁴Department of Molecular Biosciences, The University of Texas at Austin, Austin, TX 78712, USA

⁵Department of Pathology, Microbiology and Immunology, Vanderbilt University Medical Center, Nashville, TN 37232, USA

⁶Department of Microbiology, Tumor and Cell Biology, Karolinska Institutet, Stockholm, Sweden

Vaccine Research Center, National Institute of Allergy and Infectious Diseases, National Institutes of Health, Bethesda, MD, USA

⁸Florida Research and Innovation Center, Cleveland Clinic, Port Saint Lucie, FL 34987, USA

⁹Institute for Biomedicine and Glycomics, Griffith University, Gold Coast Campus, Gold Coast, QLD, Australia

¹⁰Division of Allergy and Infectious Diseases, University of Washington School of Medicine, Seattle, WA, USA

¹¹Vanderbilt Institute for Infection, Immunology and Inflammation, Vanderbilt University Medical Center, Nashville, TN 37232, USA

¹²Department of Computer Science, Vanderbilt University, Nashville, TN, USA

¹³Center for Structural Biology, Vanderbilt University, Nashville, TN, USA

¹⁴Department of Biomedical Informatics, Vanderbilt University Medical Center, Nashville, TN 37232, USA

¹⁵Department of Chemical and Biomolecular Engineering, Vanderbilt University, Nashville, TN, USA

¹⁶Department of Biochemistry, Vanderbilt University School of Medicine, Nashville, TN 37237, USA

¹⁷Lead contact

^{*}Correspondence: ivelin.georgiev@vumc.org https://doi.org/10.1016/j.cell.2025.10.006





provide variable genes and framework regions for the antibody. Additionally, such models are primarily structure-based and require antibody-antigen complexes for training, which is significantly limiting due to insufficient data, especially in the context of paired, human antibodies.

In this manuscript, we present MAGE (monoclonal antibody generator), a protein language model (PLM) capable of generating paired heavy- and light-chain antibody-variable sequences with binding specificity against input antigen sequences. MAGE was developed by fine-tuning Progen2, an auto-regressive decoder LLM that was pretrained on general protein sequences. Progen2 learns from observed amino acid sequences by next-token prediction, using self-attention to capture complex dependencies within input sequences. Here, we leveraged this pretrained model's learned representation of amino acid sequences as a starting point for learning human antibody sequence features associated with binding specificity to diverse antigen targets. We show that MAGE is capable of generating antibodies that exhibit diverse sequence features, including heavy- and light-chain variable gene usage, levels of somatic hypermutation (SHM), and novel CDRs not observed in the training data. When prompted with SARS-CoV-2 wild-type receptor binding domain (RBD), binding specificity was successfully confirmed for 9/20 of experimentally validated MAGE-generated antibodies, including one antibody with better than 10 ng/mL potency of SARS-CoV-2 neutralization. Binding antibodies were also designed and validated against respiratory syncytial virus A (RSV-A) prefusion F (7/23 antibodies), which was significantly less represented in the training data. We determined a cryo-electron microscopy (cryo-EM) structure of two MAGE-designed antibodies in complex with RSV F, demonstrating that MAGE generates antibodies with diverse binding modes and can incorporate impactful residues at key binding interfaces. Finally, MAGE-designed antibodies were validated against H5/TX/24 hemagglutinin (HA) (5/18 antibodies), demonstrating zero-shot learning capabilities against an influenza virus strain that was not present in the training data. MAGE therefore represents a first-in-class model capable of designing novel human antibodies with demonstrated functionality against antigen targets of interest, without having to provide any part of the antibody sequence as a starting template.

RESULTS

Fine-tuning a PLM for antigen-specific antibody generation

Here, we present a PLM called MAGE, fine-tuned for generating paired heavy- and light-chain antibody-variable sequences that bind to a prompted antigen sequence. Toward this goal, the pretrained model Progen2⁷ was fine-tuned on a training database of 18,507 antibody-antigen sequence pairs curated from literature and existing databases (Figure 1A). The largest group of sequences were sourced from the coronavirus antibody database (CoV-AbDab),⁸ from which 10,043 human antibodies with published heavy- and light-chain sequences were selected (Figure S1A), then mapped back to their cognate antigen sequences based on reported binding specificities. In addition, sequences for antibody-antigen pairs across a diverse range of

antigens were pulled from the structural antibody database (SAbDab)⁹ (n=2,113) and the patent and literature antibody database (PLAbDab)¹⁰ (n=987). Finally, antibody sequences were manually curated from literature containing high-throughput quantitative binding data for paired antibody sequences (n=2,030). ^{11–23}

In addition to published data, we collected an original dataset of antigen-specific antibody sequences against diverse viral antigens using LIBRA-seq (linking B cell receptors to antigen-specificity through sequencing), a high-throughput method for identification of antigen-specific B cell receptors (BCRs) against an antigen panel. A panel of 18 diverse antigens was used to screen peripheral blood mononuclear cells (PBMCs) from 20 donors distributed across four groups (HIV-infected, influenza-vaccinated, COVID-19-convalescent, and healthy). After filtering based on LIBRA-seq scores (LSSs), this dataset yielded 1,924 BCR sequences with LIBRA-seq signal for at least one antigen in the panel (Figure S1B).

In total, 67% (12,480/18,507) of the training data consist of antibodies against coronavirus (CoV)-related antigens, with 3,000 (16.2%) antibodies included against the exact wild-type RBD sequence used for prompting (Figure 1B). Of the remaining training examples, the most abundant target groups were viral antigens including influenza, RSV, and HIV-1 (Figure 1C). There were, however, 987 other training antibodies with specificities against 535 different antigens sourced from the SAbDab, many of which were not viral proteins (Table S1). Using this diverse training dataset, we aimed to present a model capable of generating functional, target-specific antibodies against input antigen sequences.

Even with the inclusion of antibody-antigen pairs from these various data sources, the training dataset was far too small to train an LLM from scratch. General protein models have been shown to have superior performance on antibody-specific tasks, due to the complex nature of understanding the input antigens, antibodies, and the interactions between them. 1,7 We therefore fine-tuned the general protein model Progen2-base, which was pretrained on over a billion protein sequences across diverse domains, for the task of antigen-specific antibody generation. This was achieved by providing antibody-antigen pairs as concatenated sequences, separated by tokens between the heavy and light chains ([LC]) and between the antibody and antigen sequences ([SEP]) (See STAR Methods section "Finetuning"; Figure S1C). Progen2-base has a context window of 2,048 tokens, well beyond the length of larger antigens including the full SARS-2 spike (1,261 residues), enabling the model to process these concatenated sequences during training.

Generated antibody sequences are diverse and distinct from training data

Following fine-tuning, the trained model could be prompted with an antigen sequence of interest to generate an output containing an antibody-variable heavy- and light-chain sequence. To evaluate the ability of MAGE to generate antigen-specific antibody sequences, we selected three targets that span the range of training data representation. We first tested generation against SARS-CoV-2 RBD, which had disproportionately higher representation in the training data. Then, to show that the model





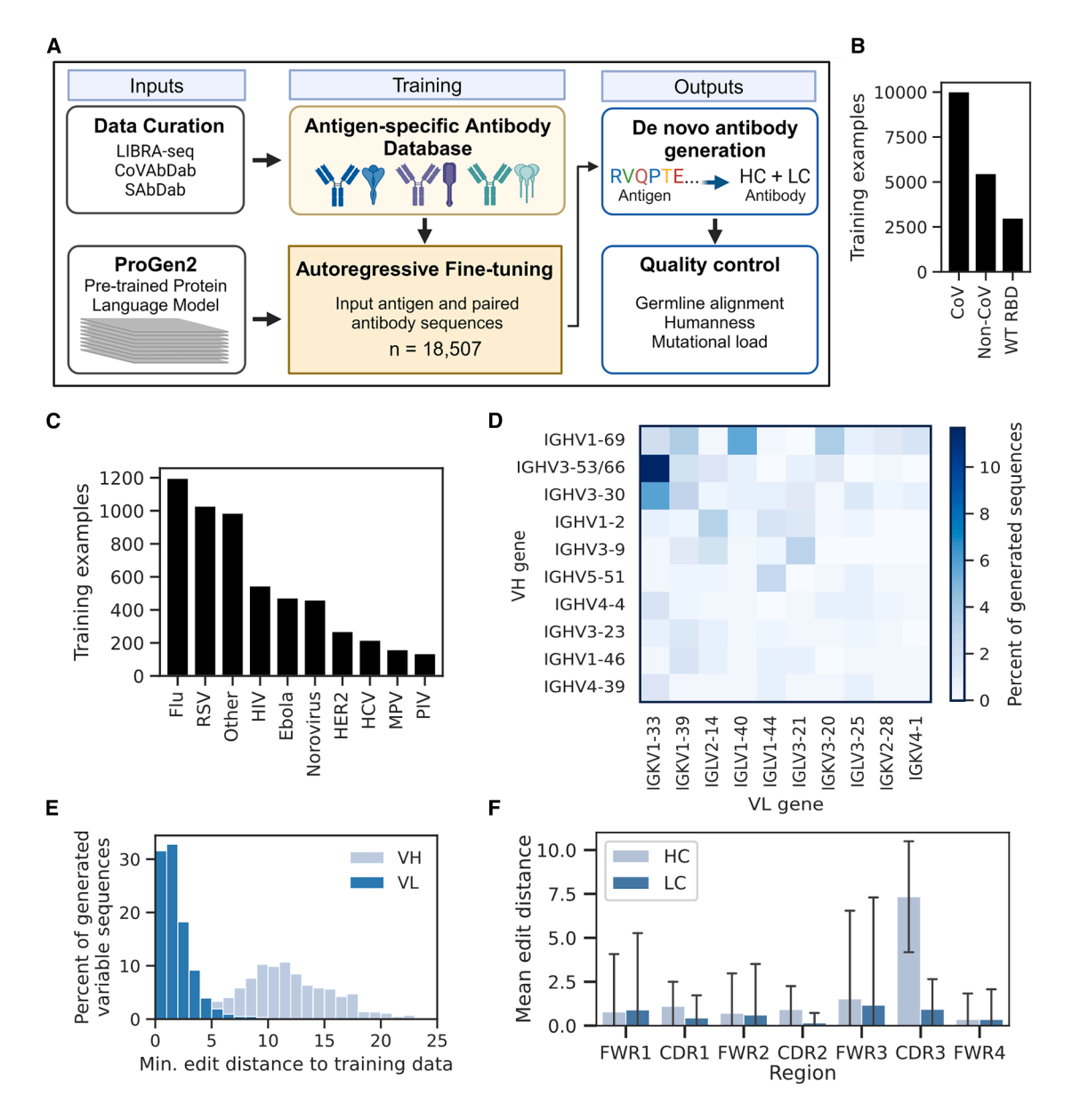


Figure 1. Progen2 was fine-tuned for antigen-specific antibody generation

(A) An antigen-specific antibody database was curated, in combination with large-scale LIBRA-seq datasets, in order to fine-tune Progen2 for paired chain antibody generation against antigen prompts.

- (B) Counts of antibody-antigen pairs in training database, grouped by CoV specificity.
- (C) Training counts of non-CoV antigen groups.
- (D) Percentage of 1,000 antibodies generated against RBD that use each combination of heavy and light V genes. The top-10 most-common genes are shown for each.
- (E) Generated variable heavy (VH) and variable light (VL) sequences were aligned to the training data to find the minimum number of mutations between each generated sequence and any training sequence.
- (F) For the most similar training sequence from the comparison in (C), the distance was calculated between each region of the VH or VL sequence. The mean across all RBD-generated sequences are shown with error bars representing the standard deviation.

 See also Figure S1 and Table S1.

can successfully work for antigen targets with less training data, we tested against two additional antigens. To assess the quality and diversity of sequences generated by MAGE, 1,000 antibody sequences were generated against RBD and aligned to a human

germline reference using IMGT numbering,²⁴ and then filtered using the following criteria (described in detail in STAR Methods): (1) removal of sequences without a recognizable heavy or light chain, (2) removal of sequences with any missing





CDRs or framework regions (FWRs), and (3) removal of variable heavy or light sequences fewer than 100 amino acids (aa) in length. Almost all (991/1,000) of the generated sequences passed these filters. Additionally, sequences were scored for "humanness" using the open source platform BioPhi OASis. Based on suggested thresholds, sequences with an OASis percentile score less than 70% were removed, with only 2.2% (22/991) sequences falling below this humanness threshold (Figure S1D). While these sequences could represent viable, particularly novel sequences, this model was intended to generate human antibodies for further characterization, and these low-scoring antibodies by OASis were removed accordingly. In total, 969 of 1,000 generated sequences were retained for further analysis and down-selection for *in vitro* characterization.

The RBD-prompted sequences displayed diverse sequence features, using 37 unique variable heavy-chain genes and 30 unique variable light-chain genes, not accounting for different alleles. In total, 322 different pairs of heavy and light variable genes were represented in the generated sequences, with the most frequently used pair (IGHV3-53/66: IGKV1-33) representing only 13.9% (135/969) of sequences (Figure 1D). Generated sequences also show diverse CDRs, with heavy-chain CDR3 (CDRH3) lengths ranging from 5 to 28 aa (mean = 16), and light-chain CDR3s (CDRL3) lengths ranging from 7 to 12 aa (mean = 10) (Figure S1E). The light chains were more biased toward germ line, with 50.1% (486/969) of containing no mutations, compared with 18.1% (175/969) for the heavy chains (Figure S1F). These results suggest that rather than simply using a single dominant heavy-light chain combination, MAGE is capable of generating diverse populations of antibody sequences.

We next sought to determine the novelty of generated antibodies at an individual level. In an attempt to quantify this novelty, each generated sequence was compared to all sequences seen during fine-tuning to identify the most similar training example, based on the minimum Levenshtein distance between each pair of sequences. This distance, which can be intuitively interpreted as the number of amino acid differences, was first calculated separately for the heavy and light chains (Figure 1E). We observed that the generated heavy chains contained more differences from training data sequences on average (mean = 11.7 differences), compared with light chains, which exhibited substantially lower levels of differences (mean = 1.4 differences). When separated based on antibody sequence region, the distances to the nearest training sequence were highest in the CDR3s (Figure 1F), as could be expected due to the high diversity in this region. Distances were higher for the heavy chains than light chains across all regions, aside from framework region 4 (FWR4). We also compared the similarity of generated heavychain CDRH3s specifically to the training RBD sequences by finding the maximum sequence identity based on Levenshtein distance. The generated CDRH3s were largely novel, covering a range of identities centered at a mean of 72.4% sequence identity, with 7.4% of the generated antibodies containing CDRH3s identical to an antibody seen in training (Figure S1G). The distribution of similarity to training data based on both heavy- and light-chain distance and CDR3 identity was broad (Figure S1H), suggesting that the generated antibody sequences cover a range of uniqueness with respect to sequences seen in training. Together, these results indicate that MAGE-generated sequences with differences in all regions of the antibody, rather than only designing CDRs.

Generated antibodies exhibit diverse binding profiles to SARS-CoV-2 RBD

Following basic filtering of the 1,000 generated antibody sequences, we used a simple pipeline to select antibodies for experimental validation of binding (Figure 2A). From the 969 antibody sequences that remained after filtering, 10 antibodies were first chosen in an unbiased manner, without comparison against RBD-specific antibodies. To test a diverse unbiased set, the 20th and 80th percentile of variable heavy (VH) germline identity antibodies from sequences using the top 5 most frequently generated VH genes were selected. Another set of 10 antibodies was selected based on similarity to known RBD-specific antibodies. For this biased selection, the top 5 antibodies with the highest CDRH3 identity to any CoV-AbDab antibody, and the top 5 antibodies with the highest VH identity to any CoV-AbDab antibody, were chosen. In total, a set of 20 antibodies was selected for in vitro validation, containing a range of sequence characteristics and novelty that aimed to represent the distribution of generated sequences (Table S2). When compared to the most similar training antibody, the selected antibodies ranged from a minimum VH distance of 3 residues (RBD-238) to 24 different residues (RBD-153) (Figure 2B). The respective light chains were more similar to those seen in training, with a minimum distance ranging from 0 residues (RBD-135) to 9 residues (RBD-727).

The 20 antibodies selected for experimental validation were tested for binding to RBD from the SARS-CoV-2 index strain by ELISA (enzyme-linked immunosorbent assay) (Figures 2C and S2A-S2D). From these results, 9/20 (45%) of the tested antibodies were identified as binding hits for further characterization, based on a minimum of 2-fold signal over background at the highest antibody concentration tested (10 µg/mL). In the biased-selection group, 2/5 of the CDRH3 matches (RBD-159, RBD-951) and 4/5 of the VH matches (RBD-238, RBD-409, RBD-413, and RBD-446) displayed binding by ELISA. In the unbiased-selection group, 3/10 antibodies (RBD-61, RBD-404, and RBD-839) displayed binding, with RBD-839 displaying a strong binding signal, on par with the positive control antibody S309.²⁶ All of these binding antibodies show no detectable ELISA signal to BG505, an HIV-1 envelope trimer. While the binding antibodies generally exhibited lower minimum distances from both VH and VL (variable light) training sequences compared to the antibodies that showed no binding, the binding antibodies nevertheless exhibited substantial novelty, with a range of 5-25 (mean 13.6) total distance to closest training antibody (Figure 2D). In particular, RBD-839 showed a higher minimum distance from the nearest training antibody (total distance = 18 residues) than 67% of the non-binding antibodies (Figure 2D). We observed a wider range of VH distances to training data compared with VL, in alignment with the lower diversity of light chains we previously observed in the pool of generated antibodies and training data.





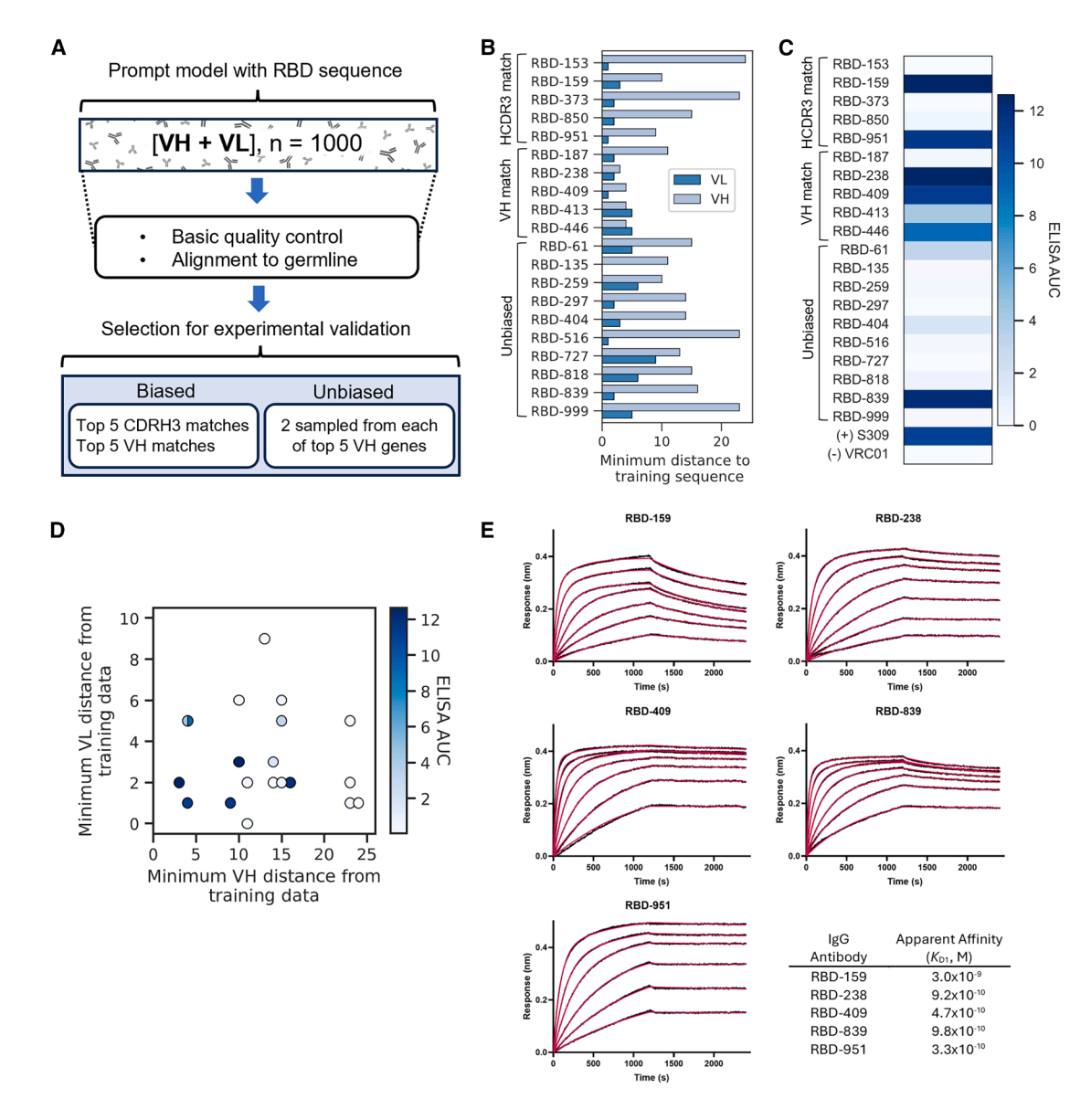


Figure 2. Twenty antibodies were selected for experimental validation of binding to RBD

(A) Schematic of antibody selection method after generation, yielding a total of 20 antibodies for experimental validation.

(B) For each antibody, the Levenshtein distance for the VH or VL is shown in comparison to the training antibody with the lowest total distance (summed across VH and VL). Antibodies are grouped by selection group.

(C) ELISA area under the curve (AUC) based on absorbance at 450 nm across a dilution series from 6.4×10^{-4} to 10 $\mu g/mL$, with S309 (RBD-specific) positive control and VRC01 (HIV-1-specific) negative control antibodies.

(D) Relationship between the minimum VH and VLs distance from the closest training antibody sequences with points colored based on ELISA AUC. Overlapping points at VH distance = 4 and VL distance 5 are shown a single point, with split coloring based on AUCs of these two antibodies (RBD-446, RBD-413).

(E) BLI sensorgrams for binding of high-affinity IgG antibodies to immobilized SARS-CoV-2 RBD-SD1. Data (black) were fitted to a 1:2 bivalent analyte model. Curve fits are shown in red. More extensive kinetics are shown in Figures S2E–S2G. See also Figure S2 and Table S2.

Binding was further validated using biolayer interferometry (BLI) to measure association and dissociation kinetics for immunoglobulin G (IgG) binding to immobilized, monomeric SARS-CoV-2 RBD (RBD-SD1) (Figures 2E and S2E). Apparent K_D (K_{D1}) values were determined by fitting the resulting binding curves to a 1:2 bivalent analyte model, ²⁷ which accounts for

the slower observed dissociation rate due to avidity. Of the hits identified by ELISA, 8 of 9 demonstrated measurable binding to RBD-SD1, with no binding observed for RBD-404 at the highest concentration tested (1,024 nM). Four antibodies from the biased-selection groups (RBD-159, RBD-238, RBD-409, and RBD-951) and one from the unbiased-selection group





(RBD-839) demonstrated apparent high-affinity binding, with K_{D1} values in the nanomolar to sub-nanomolar range. RBD-61, RBD-413, and RBD-446 also bound to RBD-SD1, albeit with reduced apparent affinity (Figure S2F). Although a small amount of non-specific binding was detected for one antibody (RBD-951), for the other 7/8 antibodies no binding was observed by BLI to a prefusion-stabilized RSV F trimer (DS-Cav1²⁸), which is consistent with the specificity observed by ELISA (Figure S2G).

Although Figure 2D shows that the antibody sequences are distinct from the training data, exhibiting a range of novelty, we sought to assess how similar the generated binding antibodies are at the population level. Public antibody clones, commonly defined by matching variable genes and CDR3 identity >70%, represent a set of criteria for grouping similar antibodies found in different individuals that are likely to share the same binding specificity.²⁹⁻³¹ When comparing the generated binding antibodies to antibodies from the CoV-AbDab using this definition, we found a range of "publicness," from zero public clones for RBD-61 and RBD-404 to the highly public RBD-238 with over 100 public clones (Figure 3A). We observed that all generated binding antibodies had >70% CDRH3 identity with at least one CoV-AbDab antibody, which is not surprising given the vast diversity and size of the database. Some of these antibodies, e. g., RBD-951, shared sequence features with many training antibodies at a population level, while others, e.g., RBD-61, appeared much less public (Figure S3A). When comparing each generated binding antibody to its closest training match based on VH distance, we observed that the majority of differences were in the CDRH3, but almost all (8/9) of the binding antibodies contained at least one difference outside of the CDRH3 (Figure 3B), demonstrating the ability of MAGE to generate distinct full variable sequences rather than only designing CDRs. In addition to varying levels of publicness and locations of mutations, we demonstrated that RBD-specific antibodies generated by MAGE have diverse sequence features including CDR lengths, variable gene usage, and humanness scores (Figure 3C).

Generated RBD antibodies bind full-length spike and neutralize SARS-CoV-2

The 9 binding antibodies to RBD were tested for binding to full-length SARS-CoV2 spike (index), along SARS-CoV spike (SARS-CoV-1) and the zoonotic Betacoronavirus Lyra-CoV. Although MAGE was prompted using RBD only, we wanted to interrogate whether the generated antibodies would be compatible with and bind full-length spike. Of the RBD-binding antibodies, 6/9 showed binding to full-length spike in ELISA (Figure 3D), suggesting that the subset of RBD-specific but non-spike-binding antibodies may bind epitopes that are occluded or bind in conformations that may be sterically hindered on the spike trimers. Two of these antibodies (RBD-951 and RBD-839) also displayed a weak signal to SARS-CoV-1 and Lyra-CoV spikes (Figure S3B). These results further emphasize that MAGE was able to generate antibodies with diverse characteristics and binding properties, exhibiting cross-reactivity to different coronavirus spike variants.

Following validation of binding by ELISA, we aimed to determine whether the generated antibodies also exhibited virus neutralization in a pseudovirus assay.³¹ Four of the RBD-binding

antibodies displayed neutralization against SARS-CoV-2 index pseudovirus, with RBD-409 displaying highly potent neutralization (IC $_{50}$ = 6.7 ng/mL) (Figures 3E and S3C). Out of the 6 antibodies that bound full spike in ELISA, all but one showed neutralization potency of <1 μ g/mL against at least one spike variant. None of these antibodies were able to neutralize XBB.1.5, although this was unseen in training as the newest RBD variant included in training was Omicron BA.5. Nevertheless, RBD-409 displayed high neutralization potency against the SARS-CoV-2 spike Gamma (IC $_{50}$ = 17 ng/mL) and Delta (IC $_{50}$ = 4.1 ng/mL) variants and was able to retain neutralization against several Omicron variants including BA.2, BA.2.75, and BJ.1 (Figure 3F).

MAGE is capable of generating functional antibodies against diverse targets with lower representation in the training datasets

While the training dataset used to fine-tune MAGE was highly biased toward coronavirus antibody-antigen pairs, the dataset did contain other diverse antigen specificities to enable generation against different prompts. To that end, antibodies were designed and tested for binding against a newly emerging, highly pathogenic avian influenza virus³² (H5) and the RSV-A glycoprotein prefusion F (RSV-A). For RSV-A, there were 292 training antibodies against the exact RSV F sequence used for prompting, along with 753 antibodies against related RSV antigens, including RSV-B and postfusion RSV F. Hence, the number of exact prompt training antibodies for RSV-A represented approximately 1/10 of the size of the training antibodies for SARS-CoV-2 RBD. In addition to validating antibody designs against a target with limited training data, we also sought to test the capability of MAGE to generate antibodies against a target not seen in training (zero-shot). Toward this goal, we prompted MAGE using HA from the avian influenza (H5N1 clade 2.3.4.4b virus), an emerging public health threat with multiple reported interspecies transmissions, including human infections. 32,33 While this exact antigen sequence was not seen in training and was not even reported at the time of training MAGE, a total of 472 H5N1-specific antibodies were included in training. These training antibodies were primarily specific to the HA variant A/Indonesia/05/2005,16 which has 91.5% sequence identity to the more recent H5/TX/24 (A/Texas/37/2024) used for prompting. This target therefore represents a realistic use-case, where MAGE can generate antibodies against an emerging threat without pre-existing knowledge of binding antibodies for that specific target antigen sequence.

To explore the behavior of MAGE when prompted with different antigens, 1,000 sequences were generated against H5/TX/24 HA and RSV-A F. Notably, there was a significant enrichment of RSV-A and H5-specific clones (using same VH gene and 70% CDRH3 identity) generated when prompting with the respective antigens, as opposed to prompting with SARS-CoV-2 RBD (Figure 4A). Almost all the antigen-specific clones were distinct from sequences seen in the training data, and most contain mutations throughout the VH region in addition to differences within the CDRH3, suggesting that MAGE learns from the training data to generate an enrichment of distinct, prompt-specific antibody sequences. Further, each of the three prompts yielded antibody sequences with unique distributions of





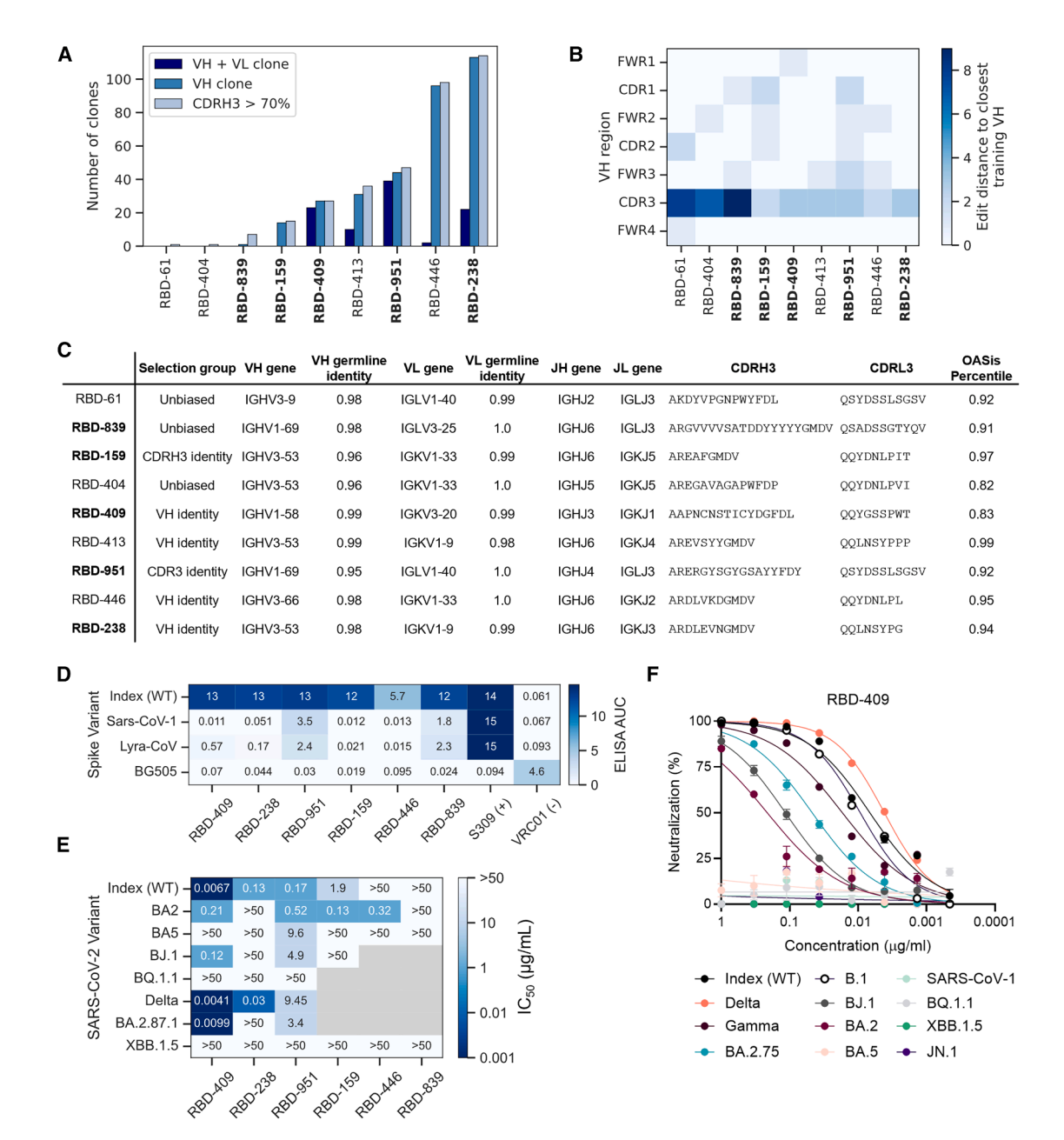


Figure 3. Generated RBD-binding antibodies have diverse sequence characteristics

(A) Publicness of binding antibodies based on CDRH3, VH, and both VH and VL. Clones defined as CDR3 identity >70% and matching V genes for the specified chain

- (B) Sum of edits within each VH region for binding antibodies compared to closest sequence match in training data.
- (C) Table showing sequence characteristics of RBD-binding antibodies. OASis percentile represents a humanness score averaged across the heavy and light chains. Strong affinity binding antibodies are bolded.
- (D) ELISA AUC for binding curve dilutions for SARS-CoV-2 WT (wild type) and other coronavirus spike variants for RBD-binding antibodies. Full ELISA dilution curves for all spike variants are shown in Figure S3B.
- E) IC_{50} values for pseudovirus neutralization of SARS-CoV-2 variants for full spike binding antibodies. Gray boxes represent strains which were not tested due to the weak neutralization of these antibodies against the index strain.
- (F) Full pseudovirus neutralization dilution curves for RBD-409 against SARS-CoV-2 variants. Data represent the percentage of neutralization as mean ± SD of two technical duplicates. Neutralization curves for all spike variants are shown in Figure S3C. See also Figure S3.



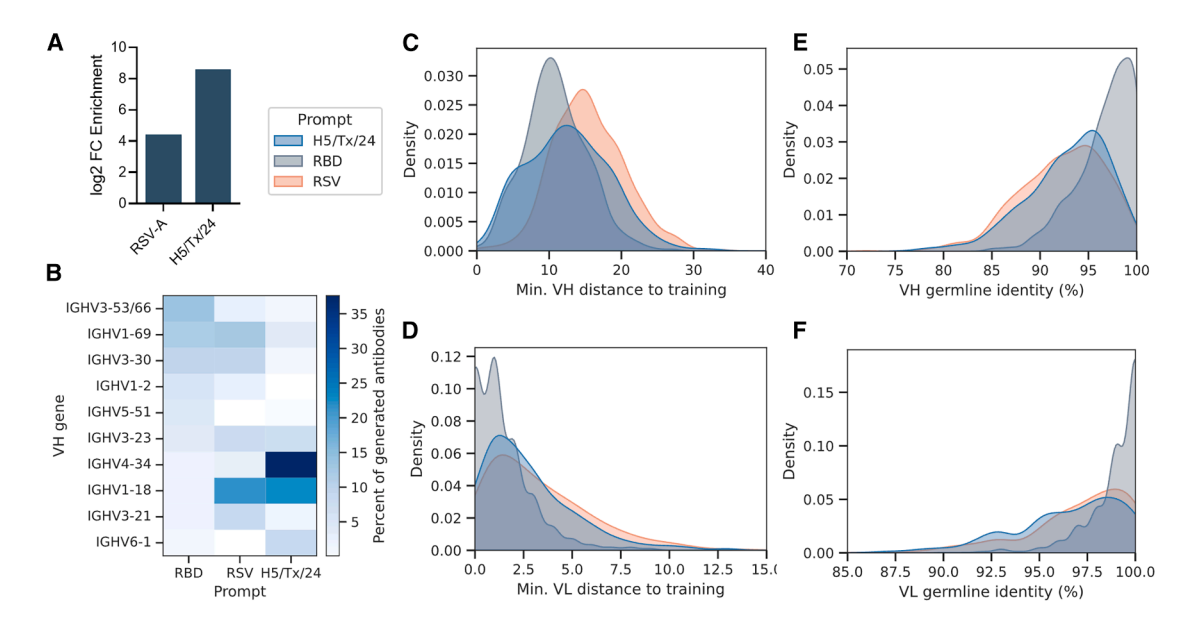


Figure 4. Characteristics of sequences generated against RSV and H5/TX/24 prompts

(A) Log fold changes showing increase in same antigen-specificity clones for RSV-A and H5/TX/24 prompts compared to WT RBD prompt. Calculated based on

number of clones between generated and training antibodies, out of 1,000 generated sequences.

(B) Heatmap showing percent of 1,000 generated antibody-encoding different variable genes for each antigen prompt.

(C–F) For 1,000 generated antibodies against each prompt, the distribution of (C) minimum VH Levenshtein distance to any training antibody, (D) minimum VL Levenshtein distance to any training antibody, (E) percent identity to VH germ line, and (F) percent identity to VL germ line.

VH gene usage, with antibodies generated with the SARS-CoV-2 RBD prompt most frequently using IGHV3-53/66, in alignment with reported gene usage biases in SARS-CoV-2-specific repertoires, ³⁴ while RSV-A sequences heavily biased toward IGHV1-18 and H5 sequences toward IGHV4-34 (Figure 4B). The antibody sequences generated against each prompt were then compared to the training data to find the minimum Levenshtein distance for each heavy and light chain, indicating that H5-and RSV-A-prompted antibodies were more novel, on average, than the RBD-prompted antibodies (Figures 4C and 4D). Additionally, we found that the H5- and RSV-A-prompted sequences exhibit higher levels of somatic hypermutation (SHM) than the RBD-prompted antibodies (Figures 4E and 4F).

We next sought to experimentally validate the binding specificity for a subset of these generated sequences against the H5 and RSV-A prompts. For H5, we compared the generated sequences to H5 training antibodies and selected a validation set of 18 designed sequences for experimental validation, aiming to capture a range of novelty compared with the training examples seen (see STAR Methods section "Antibody selection for experimental validation of H5N1 antibodies"; Table S2). We confirmed strong binding by ELISA for 5/18 (28%) of these designs (Figure 5A), along with another seven weak binding antibodies (>2-fold signal over background and >0.5 absorbance) at 10 µg/mL ELISA (Figures S4A and S4B). The minimum distance to training antibodies for the binding antibodies ranged from 4-16 residues for the heavy chain, and 1-8 residues for the light chain (Figure 5B). The levels of SHM ranged from 6%-11% for the heavy chain, and 7%-8% for the light chain (Figure 5C). Similarly to the antibodies designed against RBD,

novel residues in these H5-prompted antibodies were found across the entire VH region (Figure 5D) and were not limited to the CDRs. Notably, all 5 of the strong H5-binding antibodies were neutralizing against the influenza prompt strain A/Texas/ 37/2024 with $IC_{50} < 1$ µg/mL (Figure 5E). Additionally, these antibodies were tested against a broader panel and showed diverse neutralization patterns against H1 and H5 variants (Figure 5F).

For the RSV-A prompt, we generated a larger pool of 10,000 antibodies, followed by selection for validation of biased and unbiased selections, using a similar stratification method as used for RBD (see STAR Methods section "Antibody selection for experimental validation of RSV antibodies"), yielding a set of 23 antibodies for experimental validation of binding (Table S2). Following initial screening (Figures S4C and S4D), we confirmed binding by ELISA for 7/23 (30%) of these designs, including 3 antibodies that were selected without biasing toward known RSV-specific antibodies (Figure 6A). While the 7 binding antibodies had at least one heavy-chain clone in the training data (>70% CDRH3 identity, same VH gene), they nevertheless included many variations throughout the heavy and light chains, ranging from a minimum heavy-chain distance of six residues for RSV-6479 to 21 residues for RSV-2954 (Figure 6B). In the light chain, the distances compared to training sequences range from 4 for RSV-4314 to 12 for RSV-3301. The MAGE-designed RSV-binding antibodies show SHM levels ranging from 3%-21% for the heavy-chain, and 2%-12% for the light-chain variable region (Figure 6C), suggesting that MAGE does not simply learn germ line-level antibody sequences. Compared to the closest training antibodies, we see that the RSV-binding





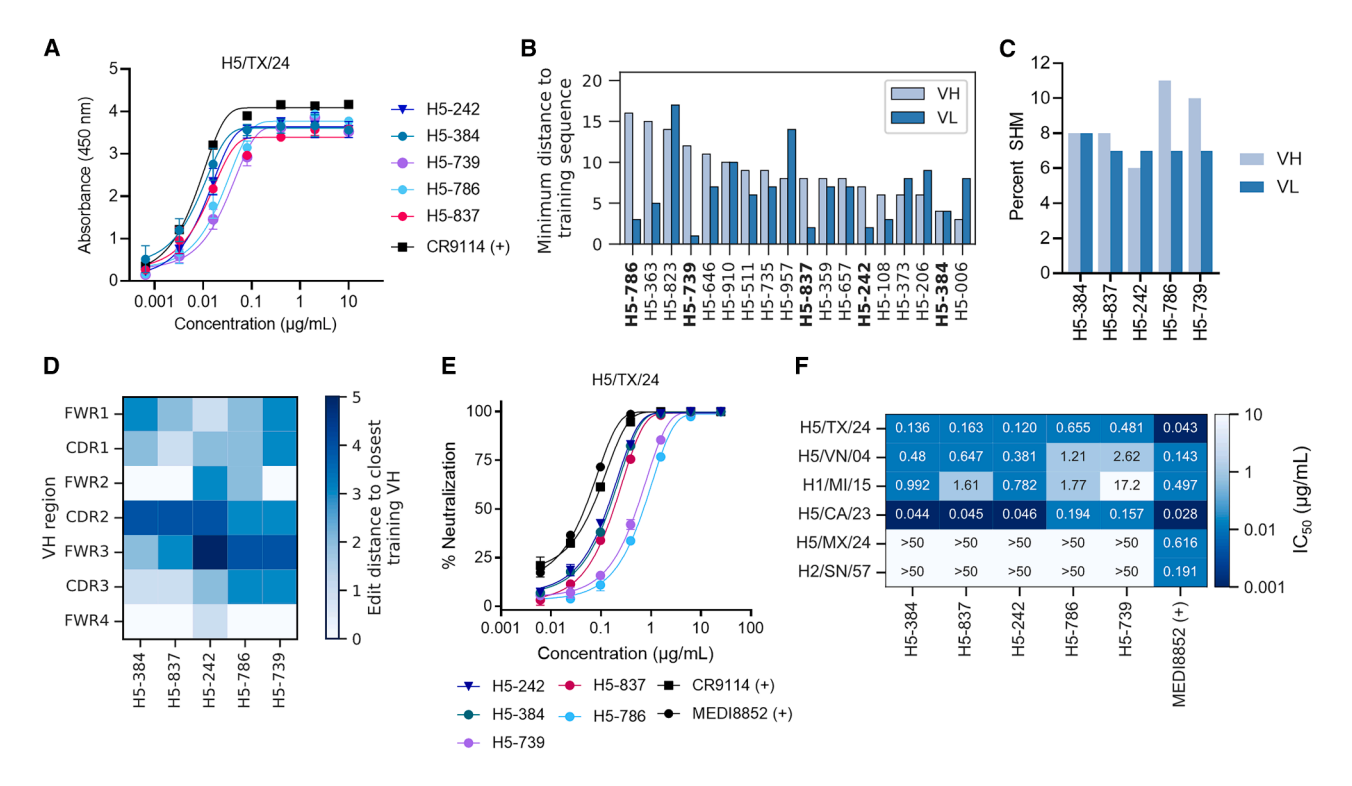


Figure 5. MAGE generates novel A/Texas/37/2024 H5-binding antibodies

(A) Full ELISA dilution curves for designed antibodies against H5/TX/24 hemagglutinin. Data are represented as means \pm SDs.

(B) Minimum distance to training antibody sequences. Distance represents number of residues different when compared to the heavy- and light-chain sequences from the training match with the lowest total distance (VH + VL).

- (C) Percent somatic hypermutation in heavy and light chain for binding antibodies, calculated across VH and VL genes.
- (D) Edit distance by VH region to closest training sequence match from (C).
- (E) Neutralization dilution curves for MAGE antibodies against H5/TX/24 hemagglutinin, with stem-binding antibodies CR9114 and MEDI8852 included as positive controls. Data are represented as means ± SDs.
- (F) IC₅₀ values for neutralization curves against different hemagglutinin strains. Full curves for neutralization breadth panel provided in Figure S4E. See also Figures S4 and S6 and Table S2.

antibodies include a range of differences across the VH regions, including differences in at least 4/7 regions for all seven binding antibodies (Figure 6D). There was also a range of novelty for the light chains in this set of antibodies, with the minimum VL distance to training antibodies ranging from 4–12 residues. The binding antibodies were further characterized by pseudovirus neutralization assays (Figures 6E and S4E). Notably, 3/7 of the binding antibodies were able to strongly neutralize RSV-A (Figure 6E), with RSV-4314 and RSV-2245 showing potent neutralization (IC $_{50} < 0.1\,\mu\text{g/mL}$). Notably, RSV-2245 was from the unbiased-selection group, with a VH distance of 17 aa to the closest training antibody and a SHM level of 10%, representing a highly mutated antibody with a notably distinct sequence. The unbiased antibody RSV-3301 also displayed some, albeit weak, neutralization.

To investigate the epitopes targeted by MAGE-generated antibodies from the unbiased-selection group with both high levels of SHM and high distances from training, we determined a cryo-EM structure of RSV prefusion F (PR-DM³⁶) bound to fragments of antigen binding (Fabs) for RSV-2245 and RSV-3301 (Figures 7A and S7). For this complex, 140,634 particles were extracted from 1,323 micrographs to generate a 3.4-Å resolution reconstruction with 3 copies of each Fab bound to the RSV F trimer.

The structure revealed that RSV-2245 binds to an epitope primarily within prefusion-specific antigenic site V, burying 850 Å² on a single F protomer. Antibodies that target site V are common in the human repertoire and tend to be potently neutralizing, 11 consistent with the neutralization efficacy we observed for RSV-2245. RSV preF is contacted by all three CDRs of the RSV-2245 heavy chain and CDRs 1 and 2 of the light chain (Figures 7B and 7C). The interface is centered on the strands of the β3-β4 hairpin, with a large network of hydrophobic contacts mediated by CDRH3 and Tyr53 of CDRH2. The sidechain of Tyr53_{CDRH2} additionally contacts a single residue within β2, forming a hydrogen bond with the sidechain of Tyr53_F. The RSV-2245 light chain contributes additional interactions within $\beta4$ and with residues that flank the $\beta3-\beta4$ hairpin. Of note, $\mbox{Asp30}_{\mbox{CDRL1}},$ which is mutated from asparagine in the germline sequence, forms a salt bridge with the Lys192_F sidechain. This mutation was only observed in 1/292 (0.34%) of the training RSV-specific antibodies, with the corresponding training antibody showing low similarity (73% LCDR1 identity and only 50% CDRH3 identity), demonstrating the ability of the model to learn sequence features from individual training sequences and integrate them into novel antibodies. The RSV-2245 epitope



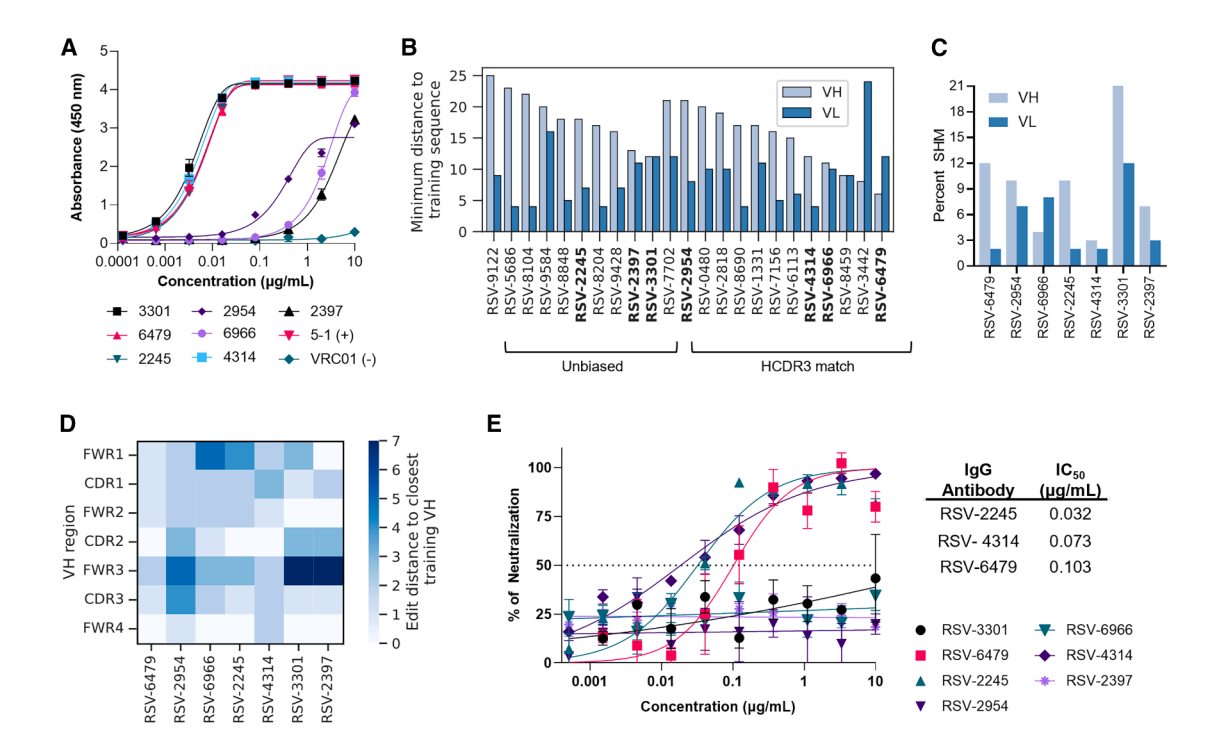


Figure 6. MAGE generates novel RSV-A binding antibodies

(A) Full ELISA dilution curves for designed antibodies against RSV-A prefusion using potently neutralizing antibody 5–1³⁵ as a positive control. Data are represented as means ± SDs.

(B) Minimum distance to training antibody sequences. Distance represents number of residues different when compared to the heavy- and light-chain sequences from the training match with the lowest total distance (VH + VL).

- (C) Percent somatic hypermutation in heavy and light chain for binding antibodies, calculated across VH and VL genes.
- (D) Distance by VH region to closest training sequence match.

(E) RSV-A neutralization dilution curves for binding antibodies against RSV-A, with IC_{50} (µg/mL) calculated from the dose-response curve. For neutralization curves, data are represented as means \pm SDs.

See also Figures S4-S6 and Table S2.

further extends to include residues within antigenic site II, mediated by polar contacts between CDRH2 and the helix-turn-helix formed by the $\alpha6$ and $\alpha7$ helices.

RSV-3301 represents the most highly mutated antibody of the validated RSV-specific set. The structure revealed that RSV-3301 buries approximately 715 Å² within the membrane-proximal lobe of one F protomer, targeting an epitope that lies almost entirely within antigenic site I. This site is typically considered to be postfusion F-specific but is largely conserved in both preand postfusion conformations. ^{37–39} The interaction is dominated by CDRH3, which extends into the cavity formed between the α 8 helix and the curved β -sheet formed in part by β 10, β 9, β 7, and β2 (Figures 7D and 7E). Backbone atoms within Asp99_{CDBH3} and Arg100_{CDBH3} form hydrogen bonds with the sidechains of Asn380_F and Asp344_F, respectively, bridging α 8 and β 9. Notably, $Arg100_{CDRH3}$ was observed in training antibodies but was not found in the most similar training antibody (VH distance = 12), despite having a highly similar CDRH3 (94.4% identity). CDRH1 and CDRH2 make polar and hydrophobic contacts within and proximal to the $\alpha 8$ helix, including two salt bridges formed between Arg32_{CDRH1} and Glu378_F and Asp58_{CDRH2} and Lys390_F. The RSV-3301 light chain also buries surface area on F between $\alpha 8$ and $\beta 2$,

primarily through hydrophobic contacts mediated by Tyr32_{CDRL1} and Tyr92_{CDRL3}. Additionally, CDRL1 and LFR3 contact residues within β 22, extending the RSV-3301 epitope into antigenic site IV.

Together, the structural characterization of these two antibodies demonstrates that MAGE generates antibodies with diverse binding properties. Not only do RSV-2245 and RSV-3301 target different binding sites of the RSV-A F protein, but these two antibodies display different binding properties. RSV-2245 contains binding residues distributed across both the heavy and light chains, whereas RSV-3301 binding is dominated by interactions within CDRH3. Although both antibodies contained MAGE-generated mutations in key binding residues, there were many mutations introduced into framework regions that did not interface with the antigen surface. To test the impact of these non-germline mutations, we reverted the VH genes to germ line and tested for binding by ELISA, with the germline-reverted RSV-3301 showing substantial reduction in binding by ELISA, while germline-reverted RSV-2245 retained comparable binding to its fully mutated form (Figures S5A and S5B). Further, BLI was used to characterize the binding of RSV-2245 Fab and RSV-3301 Fab to immobilized RSV-A F (Figures S5C and S5D). For RSV-2245, a 1:1 binding model was used to determine





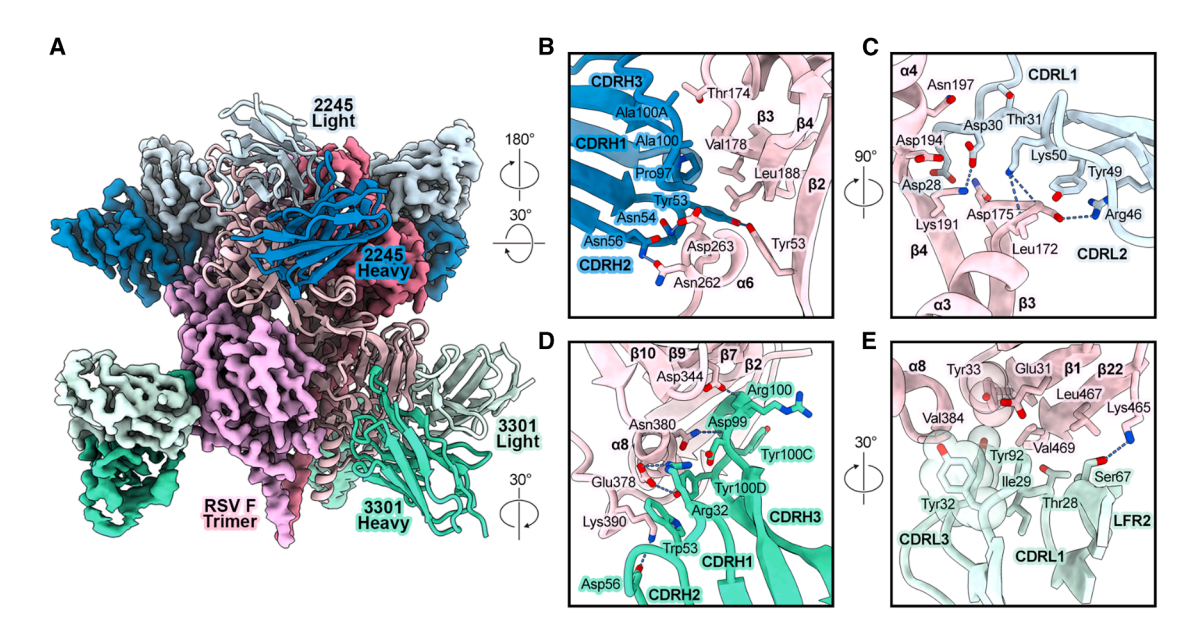


Figure 7. Cryo-EM structure of Fabs RSV-2245 and RSV-3301 bound to RSV-A F

(A–E) (A) Overview of 3.4-Å resolution cryo-EM structure of RSV F bound to fragments of antigen binding (Fabs) for RSV-2245 (heavy and light chains in dark and light blue, respectively) and RSV-3301 (heavy and light chains in dark and light green, respectively). RSV-A F protomers are shown in shades of pink. Zoomed-in views of the Fab-RSV F interface are shown as cartoons with select residues represented as sticks for (B) RSV-2245 heavy chain, (C) RSV-2245 light chain, (D) RSV-3301 heavy chain, and (E) RSV-3301 light chain. Hydrogen bonds are shown as dashed blue lines.

Details for cryo-EM data processing and structure validation are shown in Figure S7.

binding affinity ($K_D = 1.5 \times 10^{-7}$ M). Due to suspected heterogeneity in the epitope targeted by RSV-3301, these data were fitted to a heterogeneous ligand model to determine two K_D values ($K_{D1} = 6.7 \times 10^{-6}$ M and $K_{D2} = 4.5 \times 10^{-9}$ M). Together, these results show that MAGE can generate antibodies with a variety of SHM changes in different regions of the antibody sequence and with differing impacts on antigen recognition and binding affinity.

MAGE generates somatic hypermutation changes outside of consensus mutations observed in training data

Generative Al models learn patterns from example sequences seen during training, enabling the trained models to sample from learned distributions during sequence generation. While the aim of PLMs is typically to generate novel sequences, these models can reproduce common sequence features and biases seen in training.⁴⁰ In order to interrogate such biases in MAGE, generated sequences were aligned to consensus sequences constructed from the training data for each antigen target (Figures S5E-S5G). The training antibodies were grouped by heavy variable gene and target-specificity, then aligned using IMGT numbering. From this alignment, a consensus, or average, sequence was constructed by taking the most common residue at each position. Due to the high variability of the CDR3 region, this alignment was limited to the VH region consisting of framework regions 1-3 and CDRs 1 and 2. For all three targets, even though there was a population of antibodies generated with high similarity to these consensus sequences, we also observed a range of differences from consensus as high as 19 for RBD antibodies, 20 for H5 antibodies, and >40 for RSV-A antibodies (Figure S5E). While generated sequences at the higher end of these distributions have not been tested, we note that validated binding antibodies against all three targets contain examples with a distance from consensus ≥10 differences in the VH region.

For MAGE antibodies H5-384 and RSV-3301, we show a more detailed breakdown of this comparison, including any residues in the VH region that are distinct from either the training consensus or germline sequences. For H5-384 (Figure S5F), the most potently neutralizing H5-specific antibody, there were 9 residues different from the consensus alignment for H5N1-specific IGHV4-34 antibodies seen in training (n = 51) and 7 mutations from germ line. For RSV-3301 (Figure S5G), the most highly mutated RSV binder, there were 11 residues different from consensus for RSV-specific IGHV2-5 training antibodies (n = 16) and 18 mutations from germ line. Notably, 10 of these residues were different from both the consensus and germline sequences. These comparisons to the consensus training sequences suggest that MAGE is capable of generating functional antibody sequences with residues outside of the "average" of antibodies observed in training.

MAGE antibodies are predicted to have clinically relevant developability profiles

Further applications of MAGE to develop clinically relevant monoclonal antibodies will require the generation of antibodies with desirable developability profiles. To assess the MAGE antibodies presented here, the *in silico* therapeutic antibody profiler (TAP) tool was used to score developability risk profiles compared to post Phase-I clinical-stage therapeutic antibodies. TAP calculates five metrics: total CDR length,





patches of surface hydrophobicity, patches of positive charge, patches of negative charge, and structural Fv charge symmetry parameter, along with recommended thresholds based on percentiles of these metrics for the clinical-stage antibody dataset. In Figure S5H, each of the binding antibodies designed by MAGE, across all three prompt groups, are shown in relation to the therapeutic distributions for each of the TAP metrics. None of the validated MAGE antibodies exceeded Red Flag (high risk) thresholds, suggesting that these antibodies all fall within the distribution of clinical-stage therapeutic antibodies for these metrics. Three antibodies from each of the prompt groups score within the Amber Flag (medium risk) regions for at least one metric, with the most common risk being an unusually long total CDR length. Three of the MAGE antibodies could not be scored using TAP as ABodyBuilder2 failed to predict structures for these antibodies. While further experimental characterization would be needed for therapeutic development, these predictions suggest that MAGE is capable of generating antibodies with clinically relevant developability profiles.

DISCUSSION

In this work, we aimed to develop a purely sequence-based model capable of generating paired heavy-light-chain antibody sequences with prompt-specific binding. Once trained, the MAGE model presented here requires no template antibody or protein structural information. When prompted with an antigen amino acid sequence, MAGE produces full human VH and VL chains, including novel designs with changes from germline sequence introduced throughout the entire variable sequences. Our results confirm that generative PLM models like MAGE are capable of the complex task of generating full paired heavyand light-chain antibody sequences, demonstrating validated binding against RBD, H5 HA, and RSV-A prefusion F. MAGEgenerated antibodies show diverse sequence characteristics and binding properties, including potent neutralization for a subset of the binding antibodies designed against each antigen. While MAGE is not conditioned on neutralization, this demonstrates the functionality of these antibodies, and validates the ability of MAGE to produce useful, clinically relevant antibodies in the context of therapeutic discovery. For RBD and RSV-A, a subset of validated, target-specific designs were selected with no bias toward known antibodies, demonstrating design of potently neutralizing antibodies without the need for a starting template antibody sequence or structure. The design of neutralizing antibodies against H5/TX/24 HA demonstrates zero-shot learning capabilities, where MAGE was able to generate antibodies against an unseen influenza strain, by training on previously characterized antibodies with specificity against a related but divergent H5N1 strain. This demonstrates a realistic usecase for this approach, where MAGE could be used to generate antibodies against an emerging health threat more rapidly than traditional antibody discovery methods that would rely on access to specialized biological materials (e.g., blood samples or antigen protein).

The antibodies designed and characterized here display a range of sequence characteristics, including differential gene usage, CDR properties, and levels of SHM. While a subset of the

validated binding antibodies have CDRH3s that are similar to those seen in training, it is well-established that individual amino acid substitutions can disrupt antibody-antigen binding, 42,43 even within non-interfacing framework regions. 44,45 As such, the ability of the model presented here to generate bindingand in some cases potently neutralizing-antibody sequences highlights the utility of generative algorithms in creating solutions that differ from those seen in the training data, while retaining antibody-antigen recognition properties. In addition to designs with low numbers of edits introduced to training antibodies, we also validated binding for more novel antibodies with >20 total amino acid differences to the most similar training examples (RSV-2245 and RSV-3301). Structural characterization of these antibodies showed that they target different sites on RSV F with different modes of binding, which utilize residues not found in the closest training antibody matches. Additionally, the site I epitope targeted by RSV-3301 is not well-characterized and, to our knowledge, this is the first structure showing a human antibody targeting this epitope in prefusion F.⁴⁶

In this work, MAGE was validated against viral antigen targets as a proof of concept. However, data generation methods are constantly improving, and large-scale efforts using highthroughput methods such as LIBRA-seq could soon yield datasets of sufficient scale for training such models to efficiently generate antibodies against diverse antigen targets beyond what is included in the training datasets. The development of these datasets, along with the subsequent experimental validation of generated antibodies that can be incorporated into training data, will enable iterative improvement of MAGE. Since applications of LLMs in other fields have shown evidence of generalization, 47-49 we anticipate that, provided enough data, models such as MAGE could be capable of learning the more general rules of residue-level interactions that govern antibodyantigen binding, with the capability to generate antibodies against completely unseen targets. Such approaches will have the potential to revolutionize the field of antibody discovery, but the generalizability of such models is yet to be proven in this context.

Limitations of the study

A limitation of the sequence-based approach presented in this work is the lack of functional data incorporated into data engineering and training. Antibody-antigen pairs were curated in a binary manner based on database annotations, binding predictions (from LIBRA-seq data), and experimental data when available (Table S1). As a result, the scope of MAGE is limited to the generation of antibodies that bind specifically to a target of interest. Currently, the model is not capable of explicitly targeting the generation of antibodies with high binding affinity or potent neutralization. While we showed that generated antibodies can achieve such functions, the generation of desired functional qualities is currently limited by candidate selection and is not guaranteed. The application of sequence-based models such as MAGE to specific targets of interest can be tailored further through the incorporation of structure and epitope or paratope information.

We emphasize that rather than aiming to redesign antibodies, MAGE is able to sample the distribution of known binding





sequences to learn complex sequence features associated with antigen-binding specificity, and then generate a pool of diverse sequences that is highly enriched for binding antibodies, providing candidates for further characterization, down-selection, and development. However, it is of interest to determine whether MAGE antibodies demonstrate functional properties comparable to the training antibodies. For 5/7 of the RSV-binding antibodies designed by MAGE, we observed neutralization patterns similar to those of the closest training matches based on CDRH3 identity, albeit in some cases the closest antibodies from training were more potent. The closest antibodies for two of the non-neutralizing MAGE antibodies (RSV-6966 and RSV-2397) show potent neutralization (IC₅₀ < 0.1 μ g/mL) (Figures S6A-S6C). This comparison was also performed for H5-specific MAGE antibodies (Figures S6D and S6E). Here, we observed that MAGE antibody H2-739 demonstrated increased neutralization specificity against H5 variants over other HA subtypes (H1 and H2) compared to its training match, which had increased neutralization breadth. H5-242 showed broader neutralization than its training match, along with increased potency against the prompt strain of H5/TX/24. These results suggest that MAGE can generate neutralizing antibodies that have diverse phenotypes that are distinct from those observed in the training data. We note that, in this study, we have only sampled a fraction of the MAGE-generated antibody sequence space for experimental validation but envision that this candidate pool could be further mined to find antibodies with improved functional properties Figure S7.

Extensive validation of MAGE designs, especially against targets with lower or no representation in the training data, is limited due to challenges related to large-scale expression, purification, and validation of antibody sequences. While we have shown that clustering and random sampling of generated sequences is sufficient to yield binding antibodies from small batches of designs against targets highly represented in the training data, we have not validated this capability in the context of novel, or unseen, targets and expect that success rates would be much lower for such cases. Even though the model presented here is currently limited by the need for further candidate down-selection, either through comparison of generated sequences to known antibodies or through the use of downstream predictive models, we anticipate that the capacity for such applications will be enabled by the incorporation of larger training datasets as libraries of antigen-specific antibody species continue to grow.

RESOURCE AVAILABILITY

Lead contact

Information and requests for reagents may be directed to, and will be fulfilled by, the lead contact, Ivelin Georgiev (ivelin.georgiev@vumc.org).

Materials availability

Reagents are available on request from the lead contact with a completed materials transfer agreement. Information on reagents used in this study is available in the key resources table.

Data and code availability

 Raw sequencing reads from LIBRA-seq have been uploaded to the National Library of Medicine Sequence Read Archive (SRA) under the

- BioProject ID SRA: PRJNA1321287 and are publicly available as of the date of publication.
- Protein Data Bank (PBD) and Electron Microscopy Data Bank (EMDB) identification numbers for the cryo-EM structure and map reported in this manuscript are listed in the key resources table and are publicly available as of the date of publication.
- Original Python scripts for using MAGE to generate antibodies, as well as the analysis of generated antibodies for the figures presented in this paper, are publicly available at https://github.com/IGlab-VUMC/MAGE_ab_generation.
- The fine-tuned weights for the MAGE model have been uploaded to HuggingFace at https://huggingface.co/perrywasdin/MAGE_V1.
- Any additional information required to reanalyze the data reported in this
 paper is available from the lead contact upon request.

ACKNOWLEDGMENTS

We thank all members of the Georgiev laboratory for their support and feedback. We thank Ben Murrell for feedback on the manuscript. We thank Vito Quaranta and Darren Tyson for providing computational resources through the Quantitative Systems Biology Center. We thank the Vanderbilt Technologies for Advanced Genomics Core (VANTAGE), which is supported in part by CTSA (5UL1 RR024975-03), for providing technical assistance with library production and sequencing. This research was funded, in part, by: Advanced Research Projects Agency for Health agreement 1AY2AX000077 (I.S.G.); G. Harold and Leila Y. Mathers Charitable Foundation grant MF-2107-01851 (I. S.G.); National Institutes of Health grants R01Al175245 and R01 Al152693 (I. S.G.) and ZIA Al005003 (M.K.); Swedish Research Council grants 2018-02381 and 2023-02516; and Welch Foundation grant F-0003-19620604 (J.S. M.). This research was supported in part by the Intramural Research Program of the National Institutes of Health (NIH) and the Advanced Research Projects Agency for Health (ARPA-H). The contributions of the NIH authors are considered Works of the United States Government. The views and conclusions contained in this document are those of the authors and should not be interpreted as representing the official policies, either expressed or implied, of the U.S. Government. We would like to thank Mark Connors for providing HIV-1 PBMC samples. Biorender was used for creating schematic figures. The funders had no role in the conceptualization or execution of the studies or drafting of the manuscript.

AUTHOR CONTRIBUTIONS

Conceptualization, P.T.W., T.M.M., and I.S.G.; methodology, P.T.W. and I.S.G.; investigation, P.T.W., N.V.J., A.K.J., J.R.K., T.M.M., G.H., T.M.R., G. J., O.C.P., M.J.V., S.H., L.V., D.J.S., R.A.G., S.F.A., M.K., G.A.S., F.P., and C.M.H.; project administration, G.H., J.L., H.Y.C., G.A.S., and T.M.R.; supervision, J.S.M., A.A.A.-S., and I.S.G.; writing—original draft, P.T.W. and I.S.G.; writing—review & editing, P.T.W., N.V.J., A.K.J., J.R.K., T.M.M., G.H., T.M. R., G.J., O.C.P., M.J.V., S.H., L.V., D.J.S., R.A.G., S.F.A., M.K., G.A.S., F.P., C.M.H., J.S.M., A.A.A.-S., and I.S.G.

DECLARATION OF INTERESTS

I.S.G. is a cofounder of AbSeek Bio. P.T.W and I.S.G. are listed as inventors on patents filed describing the pipeline presented here for the fine-tuning of LLMs for antigen-specific antibody generation. The Georgiev laboratory has received unrelated funding from Takeda and Merck. H.Y.C. has consulted for Bill and Melinda Gates Foundation and Ellume and has served on advisory boards for Vir, Merck, and AbbVie; she has received research funding from Gates Ventures and support and reagents from Ellume and Cepheid outside of the submitted work.

STAR*METHODS

Detailed methods are provided in the online version of this paper and include the following:





- KEY RESOURCES TABLE
- EXPERIMENTAL MODEL AND STUDY PARTICIPANT DETAILS
- METHOD DETAILS
 - o MAGE model development
 - o Antibody candidate validation
 - o LIBRA-seq Experiments
- QUANTIFICATION AND STATISTICAL ANALYSIS

SUPPLEMENTAL INFORMATION

Supplemental information can be found online at https://doi.org/10.1016/j.cell. 2025.10.006.

Received: February 25, 2025 Revised: July 11, 2025 Accepted: October 3, 2025

REFERENCES

- Hie, B.L., Shanker, V.R., Xu, D., Bruun, T.U.J., Weidenbacher, P.A., Tang, S., Wu, W., Pak, J.E., and Kim, P.S. (2024). Efficient evolution of human antibodies from general protein language models. Nat. Biotechnol. 42, 275–283. https://doi.org/10.1038/s41587-023-01763-2.
- Desautels, T.A., Arrildt, K.T., Zemla, A.T., Lau, E.Y., Zhu, F., Ricci, D., Cronin, S., Zost, S.J., Binshtein, E., Scheaffer, S.M., et al. (2024). Computationally restoring the potency of a clinical antibody against Omicron. Nature 629, 878–885. https://doi.org/10.1038/s41586-024-07385-1.
- Shanehsazzadeh, A., Alverio, J., Kasun, G., Levine, S., Khan, J.A., Chung, C., Diaz, N., Luton, B.K., Tarter, Y., McCloskey, C., et al. (2023). In vitro validated antibody design against multiple therapeutic antigens using generative inverse folding. Preprint at bioRxiv. 2023.2012.2008.570889. https://doi.org/10.1101/2023.12.08.570889.
- Haraldson Høie, M., Hummer, A., Olsen, T.H., Aguilar-Sanjuan, B., Nielsen, M., and Deane, C.M. (2024). AntiFold: Improved Antibody Structure-Based Design Using Inverse Folding. Preprint at arXiv, 2405.03370. https://doi.org/10.48550/arXiv.2405.03370.
- Bennett, N.R., Watson, J.L., Ragotte, R.J., Borst, A.J., See, D.L., Weidle, C., Biswas, R., Shrock, E.L., Leung, P.J.Y., Huang, B., et al. (2024). Atomically accurate de novo design of single-domain antibodies. Preprint at bioRxiv. 2024.2003.2014.585103. https://doi.org/10.1101/2024.03.14. 585103
- Shuai, R.W., Ruffolo, J.A., and Gray, J.J. (2023). IgLM: Infilling language modeling for antibody sequence design. Cell Syst. 14, 979–989.e4. https://doi.org/10.1016/j.cels.2023.10.001.
- Nijkamp, E., Ruffolo, J.A., Weinstein, E.N., Naik, N., and Madani, A. (2023). ProGen2: Exploring the boundaries of protein language models. Cell Syst. 14, 968–978.e3. https://doi.org/10.1016/j.cels.2023.10.002.
- Raybould, M.I.J., Kovaltsuk, A., Marks, C., and Deane, C.M. (2021). CoV-AbDab: the coronavirus antibody database. Bioinformatics 37, 734–735. https://doi.org/10.1093/bioinformatics/btaa739.
- Dunbar, J., Krawczyk, K., Leem, J., Baker, T., Fuchs, A., Georges, G., Shi, J., and Deane, C.M. (2014). SAbDab: the structural antibody database. Nucleic Acids Res. 42, D1140–D1146. https://doi.org/10.1093/nar/ gkt1043.
- Abanades, B., Olsen, T.H., Raybould, M.I.J., Aguilar-Sanjuan, B., Wong, W.K., Georges, G., Bujotzek, A., and Deane, C.M. (2024). The Patent and Literature Antibody Database (PLAbDab): an evolving reference set of functionally diverse, literature-annotated antibody sequences and structures. Nucleic Acids Res. 52, D545–D551. https://doi.org/10.1093/ nar/gkad1056.
- Gilman, M.S.A., Castellanos, C.A., Chen, M., Ngwuta, J.O., Goodwin, E., Moin, S.M., Mas, V., Melero, J.A., Wright, P.F., Graham, B.S., et al.

- (2016). Rapid profiling of RSV antibody repertoires from the memory B cells of naturally infected adult donors. Sci. Immunol. 1, eaaj1879. https://doi.org/10.1126/sciimmunol.aaj1879.
- Zurbuchen, Y., Michler, J., Taeschler, P., Adamo, S., Cervia, C., Raeber, M.E., Acar, I.E., Nilsson, J., Warnatz, K., Soyka, M.B., et al. (2023). Human memory B cells show plasticity and adopt multiple fates upon recall response to SARS-CoV-2. Nat. Immunol. 24, 955–965. https://doi.org/ 10.1038/s41590-023-01497-y.
- Kramer, K.J., Wilfong, E.M., Voss, K., Barone, S.M., Shiakolas, A.R., Raju, N., Roe, C.E., Suryadevara, N., Walker, L.M., Wall, S.C., et al. (2022). Single-cell profiling of the antigen-specific response to BNT162b2 SARS-CoV-2 RNA vaccine. Nat. Commun. 13, 3466. https://doi.org/10. 1038/s41467-022-31142-5.
- Shanehsazzadeh, A., McPartlon, M., Kasun, G., Steiger, A.K., Sutton, J.M., Yassine, E., McCloskey, C., Haile, R., Shuai, R., Alverio, J., et al. (2024). Unlocking de novo antibody design with generative artificial intelligence. Preprint at bioRxiv. 2023.2001.2008.523187. https://doi.org/10. 1101/2023.01.08.523187.
- Andrews, S.F., Huang, Y., Kaur, K., Popova, L.I., Ho, I.Y., Pauli, N.T., Henry Dunand, C.J., Taylor, W.M., Lim, S., Huang, M., et al. (2015). Immune history profoundly affects broadly protective B cell responses to influenza. Sci. Transl. Med. 7, 316ra192. https://doi.org/10.1126/scitranslmed. aad0522.
- Joyce, M.G., Wheatley, A.K., Thomas, P.V., Chuang, G.Y., Soto, C., Bailer, R.T., Druz, A., Georgiev, I.S., Gillespie, R.A., Kanekiyo, M., et al. (2016). Vaccine-Induced Antibodies that Neutralize Group 1 and Group 2 Influenza A Viruses. Cell 166, 609–623. https://doi.org/10.1016/j.cell.2016. 06.043.
- Weber, T., Potthoff, J., Bizu, S., Labuhn, M., Dold, L., Schoofs, T., Horning, M., Ercanoglu, M.S., Kreer, C., Gieselmann, L., et al. (2022). Analysis of antibodies from HCV elite neutralizers identifies genetic determinants of broad neutralization. Immunity 55, 341–354.e7. https://doi.org/10.1016/j.immuni.2021.12.003.
- Bornholdt, Z.A., Turner, H.L., Murin, C.D., Li, W., Sok, D., Souders, C.A., Piper, A.E., Goff, A., Shamblin, J.D., Wollen, S.E., et al. (2016). Isolation of potent neutralizing antibodies from a survivor of the 2014 Ebola virus outbreak. Science 351, 1078–1083. https://doi.org/10.1126/science. aad5788.
- Setliff, I., Shiakolas, A.R., Pilewski, K.A., Murji, A.A., Mapengo, R.E., Janowska, K., Richardson, S., Oosthuysen, C., Raju, N., Ronsard, L., et al. (2019). High-Throughput Mapping of B Cell Receptor Sequences to Antigen Specificity. Cell 179, 1636–1646.e15. https://doi.org/10.1016/ i.cell.2019.11.003.
- Walker, L.M., Shiakolas, A.R., Venkat, R., Liu, Z.A., Wall, S., Raju, N., Pilewski, K.A., Setliff, I., Murji, A.A., Gillespie, R., et al. (2022). High-Throughput B Cell Epitope Determination by Next-Generation Sequencing. Front. Immunol. 13, 855772. https://doi.org/10.3389/fimmu.2022.855772.
- Chen, E.C., Gilchuk, P., Zost, S.J., Ilinykh, P.A., Binshtein, E., Huang, K., Myers, L., Bonissone, S., Day, S., Kona, C.R., et al. (2023). Systematic analysis of human antibody response to ebolavirus glycoprotein shows high prevalence of neutralizing public clonotypes. Cell Rep. 42, 112370. https://doi.org/10.1016/j.celrep.2023.112370.
- Shiakolas, A.R., Kramer, K.J., Johnson, N.V., Wall, S.C., Suryadevara, N., Wrapp, D., Periasamy, S., Pilewski, K.A., Raju, N., Nargi, R., et al. (2022). Efficient discovery of SARS-CoV-2-neutralizing antibodies via B cell receptor sequencing and ligand blocking. Nat. Biotechnol. 40, 1270–1275. https://doi.org/10.1038/s41587-022-01232-2.
- Shiakolas, A.R., Kramer, K.J., Wrapp, D., Richardson, S.I., Schäfer, A., Wall, S., Wang, N., Janowska, K., Pilewski, K.A., Venkat, R., et al. (2021). Cross-reactive coronavirus antibodies with diverse epitope specificities and Fc effector functions. Cell Rep. Med. 2, 100313. https://doi. org/10.1016/j.xcrm.2021.100313.
- Lefranc, M.P., Giudicelli, V., Ginestoux, C., Jabado-Michaloud, J., Folch,
 G., Bellahcene, F., Wu, Y., Gemrot, E., Brochet, X., Lane, J., et al.

Cell Article



- (2009). IMGT, the international ImMunoGeneTics information system. Nucleic Acids Res. 37, D1006–D1012. https://doi.org/10.1093/nar/gkn838.
- Prihoda, D., Maamary, J., Waight, A., Juan, V., Fayadat-Dilman, L., Svozil, D., and Bitton, D.A. (2022). BioPhi: A platform for antibody design, humanization, and humanness evaluation based on natural antibody repertoires and deep learning. mAbs 14, 2020203. https://doi.org/10.1080/19420862. 2021.2020203.
- Pinto, D., Park, Y.-J., Beltramello, M., Walls, A.C., Tortorici, M.A., Bianchi, S., Jaconi, S., Culap, K., Zatta, F., De Marco, A., et al. (2020). Crossneutralization of SARS-CoV-2 by a human monoclonal SARS-CoV antibody. Nature 583, 290–295. https://doi.org/10.1038/s41586-020-2349-y.
- Apiyo, D. (2022). Biomolecular Binding Kinetics Assays on the Octet® BLI. https://www.sartorius.com/resource/blob/742330/05671fe2de45d16bd7 2b8078ac28980d/octet-biomolecular-binding-kinetics-application-note-4014-en-1-data.pdf.
- McLellan, J.S., Chen, M., Joyce, M.G., Sastry, M., Stewart-Jones, G.B.E., Yang, Y., Zhang, B., Chen, L., Srivatsan, S., Zheng, A., et al. (2013). Structure-based design of a fusion glycoprotein vaccine for respiratory syncytial virus. Science 342, 592–598. https://doi.org/10.1126/science.1243283.
- Chen, E.C., Gilchuk, P., Zost, S.J., Suryadevara, N., Winkler, E.S., Cabel, C.R., Binshtein, E., Chen, R.E., Sutton, R.E., Rodriguez, J., et al. (2021). Convergent antibody responses to the SARS-CoV-2 spike protein in convalescent and vaccinated individuals. Cell Rep. 36, 109604. https:// doi.org/10.1016/j.celrep.2021.109604.
- Setliff, I., McDonnell, W.J., Raju, N., Bombardi, R.G., Murji, A.A., Scheepers, C., Ziki, R., Mynhardt, C., Shepherd, B.E., Mamchak, A.A., et al. (2018). Multi-Donor Longitudinal Antibody Repertoire Sequencing Reveals the Existence of Public Antibody Clonotypes in HIV-1 Infection. Cell Host Microbe 23, 845–854.e6. https://doi.org/10.1016/j.chom.2018. 05.001.
- Wall, S.C., Suryadevara, N., Kim, C., Shiakolas, A.R., Holt, C.M., Irbe, E.B., Wasdin, P.T., Suresh, Y.P., Binshtein, E., Chen, E.C., et al. (2023). SARS-CoV-2 antibodies from children exhibit broad neutralization and belong to adult public clonotypes. Cell Rep. Med. 4, 101267. https://doi.org/10. 1016/j.xcrm.2023.101267.
- Uyeki, T.M., Milton, S., Abdul Hamid, C., Reinoso Webb, C., Presley, S.M., Shetty, V., Rollo, S.N., Martinez, D.L., Rai, S., Gonzales, E.R., et al. (2024). Highly Pathogenic Avian Influenza A(H5N1) Virus Infection in a Dairy Farm Worker. N. Engl. J. Med. 390, 2028–2029. https://doi.org/10.1056/ NEJMc2405371.
- Medina-Armenteros, Y., Cajado-Carvalho, D., das Neves Oliveira, R., Apetito Akamatsu, M., and Lee Ho, P. (2024). Recent Occurrence, Diversity, and Candidate Vaccine Virus Selection for Pandemic H5N1: Alert Is in the Air. Vaccines 12, 1044. https://doi.org/10.3390/vaccines12091044.
- 34. Yuan, M., Liu, H., Wu, N.C., Lee, C.D., Zhu, X., Zhao, F., Huang, D., Yu, W., Hua, Y., Tien, H., et al. (2020). Structural basis of a shared antibody response to SARS-CoV-2. Science 369, 1119–1123. https://doi.org/10.1126/science.abd2321.
- Abu-Shmais, A.A., Guo, L., Khalil, A.M., Miller, R.J., Janke, A.K., Vukovich, M.J., Bass, L.E., Suresh, Y.P., Rush, S.A., Wolters, R.M., et al. (2024). A potently neutralizing and protective human antibody targeting antigenic site V on RSV and hMPV fusion glycoprotein. Preprint at bioRxiv. 2024.10. 31.621295. https://doi.org/10.1101/2024.10.31.621295.
- Krarup, A., Truan, D., Furmanova-Hollenstein, P., Bogaert, L., Bouchier, P., Bisschop, I.J.M., Widjojoatmodjo, M.N., Zahn, R., Schuitemaker, H., McLellan, J.S., et al. (2015). A highly stable prefusion RSV F vaccine derived from structural analysis of the fusion mechanism. Nat. Commun. 6, 8143. https://doi.org/10.1038/ncomms9143.
- López, J.A., Bustos, R., Örvell, C., Berois, M., Arbiza, J., García-Barreno, B., and Melero, J.A. (1998). Antigenic structure of human respiratory syncytial virus fusion glycoprotein. J. Virol. 72, 6922–6928. https://doi.org/10. 1128/JVI.72.8.6922-6928.1998.
- 38. Anderson, L.J., Hierholzer, J.C., Stone, Y.O., Tsou, C., and Fernie, B.F. (1986). Identification of epitopes on respiratory syncytial virus proteins

- by competitive binding immunoassay. J. Clin. Microbiol. 23, 475–480. https://doi.org/10.1128/jcm.23.3.475-480.1986.
- Rossey, I., McLellan, J.S., Saelens, X., and Schepens, B. (2018). Clinical potential of prefusion RSV F-specific antibodies. Trends Microbiol. 26, 209–219. https://doi.org/10.1016/j.tim.2017.09.009.
- Olsen, T.H., Moal, I.H., and Deane, C.M. (2024). Addressing the antibody germline bias and its effect on language models for improved antibody design. Bioinformatics 40, btae618. https://doi.org/10.1093/bioinformatics/btae618.
- Raybould, M.I.J., Turnbull, O.M., Suter, A., Guloglu, B., and Deane, C.M. (2024). Contextualising the developability risk of antibodies with lambda light chains using enhanced therapeutic antibody profiling. Commun. Biol. 7, 62. https://doi.org/10.1038/s42003-023-05744-8.
- Dougan, D.A., Malby, R.L., Gruen, L.C., Kortt, A.A., and Hudson, P.J. (1998). Effects of substitutions in the binding surface of an antibody on antigen affinity. Protein Eng. 11, 65–74. https://doi.org/10.1093/protein/11.
- Winkler, K., Kramer, A., Küttner, G., Seifert, M., Scholz, C., Wessner, H., Schneider-Mergener, J., and Höhne, W. (2000). Changing the antigen binding specificity by single point mutations of an anti-p24 (HIV-1) antibody. J. Immunol. 165, 4505–4514. https://doi.org/10.4049/jimmunol. 165.8.4505.
- Foote, J., and Winter, G. (1992). Antibody framework residues affecting the conformation of the hypervariable loops. J. Mol. Biol. 224, 487–499. https://doi.org/10.1016/0022-2836(92)91010-m.
- Klein, F., Diskin, R., Scheid, J.F., Gaebler, C., Mouquet, H., Georgiev, I.S., Pancera, M., Zhou, T., Incesu, R.-B., Fu, B.Z., et al. (2013). Somatic mutations of the immunoglobulin framework are generally required for broad and potent HIV-1 neutralization. Cell 153, 126–138. https://doi.org/10.1016/j.cell.2013.03.018.
- Rossey, I., Hsieh, C.-L., Sedeyn, K., Ballegeer, M., Schepens, B., McLellan, J.S., and Saelens, X. (2021). A vulnerable, membrane-proximal site in human respiratory syncytial virus F revealed by a prefusion-specific single-domain antibody. J. Virol. 95, e02279-20. https://doi.org/10.1128/JVI.02279-20.
- 47. Bubeck, S., Chandrasekaran, V., Eldan, R., Gehrke, J., Horvitz, E., Kamar, E., Lee, P., Lee, Y.T., Li, Y., and Lundberg, S. (2023). Sparks of artificial general intelligence: early experiments with gpt-4. Preprint at arXiv, 2303.12712. https://doi.org/10.48550/arXiv.2303.12712.
- Naveed, H., Khan, A.U., Qiu, S., Saqib, M., Anwar, S., Usman, M., Barnes, N., and Mian, A. (2023). A comprehensive overview of large language models. Preprint at arXiv, 2307.06435. https://doi.org/10.48550/arXiv. 2307.06435.
- Power, A., Burda, Y., Edwards, H., Babuschkin, I., and Misra, V. (2022).
 Grokking: generalization beyond overfitting on small algorithmic datasets.
 Preprint at arXiv, 2201.02177. https://doi.org/10.48550/arXiv.2201.02177.
- Brochet, X., Lefranc, M.P., and Giudicelli, V. (2008). IMGT/V-QUEST: the highly customized and integrated system for IG and TR standardized V-J and V-D-J sequence analysis. Nucleic Acids Res. 36, W503–W508. https://doi.org/10.1093/nar/gkn316.
- Ehrhardt, S.A., Zehner, M., Krähling, V., Cohen-Dvashi, H., Kreer, C., Elad, N., Gruell, H., Ercanoglu, M.S., Schommers, P., Gieselmann, L., et al. (2019). Polyclonal and convergent antibody response to Ebola virus vaccine rVSV-ZEBOV. Nat. Med. 25, 1589–1600. https://doi.org/10.1038/s41591-019-0602-4.
- Liu, Y., Tan, H.-X., Koutsakos, M., Jegaskanda, S., Esterbauer, R., Tilmanis, D., Aban, M., Kedzierska, K., Hurt, A.C., Kent, S.J., et al. (2019). Cross-lineage protection by human antibodies binding the influenza B hemagglutinin. Nat. Commun. 10, 324. https://doi.org/10.1038/s41467-018-08165-y.
- UniProt Consortium (2022). UniProt: the Universal Protein Knowledgebase in 2023. Nucleic Acids Res. 51, D523–D531. https://doi.org/10.1093/nar/gkac1052.





- Teufel, F., Almagro Armenteros, J.J., Johansen, A.R., Gíslason, M.H., Pihl, S.I., Tsirigos, K.D., Winther, O., Brunak, S., von Heijne, G., and Nielsen, H. (2022). SignalP 6.0 predicts all five types of signal peptides using protein language models. Nat. Biotechnol. 40, 1023–1025. https://doi.org/10. 1038/s41587-021-01156-3.
- Wolf, T., Debut, L., Sanh, V., Chaumond, J., Delangue, C., Moi, A., Cistac, P., Rault, T., Louf, R., and Funtowicz, M. (2019). Huggingface's transformers: state-of-the-art natural language processing. Preprint at arXiv, 1910.03771. https://doi.org/10.48550/arXiv.1910.03771.
- Dunbar, J., and Deane, C.M. (2016). ANARCI: antigen receptor numbering and receptor classification. Bioinformatics 32, 298–300. https://doi.org/ 10.1093/bioinformatics/btv552.
- Sheward, D.J., Kim, C., Fischbach, J., Sato, K., Muschiol, S., Ehling, R.A., Björkström, N.K., Karlsson Hedestam, G.B., Reddy, S.T., Albert, J., et al. (2022). Omicron sublineage BA.2.75.2 exhibits extensive escape from neutralising antibodies. Lancet Infect. Dis. 22, 1538–1540. https://doi. org/10.1016/S1473-3099(22)00663-6.
- Creanga, A., Gillespie, R.A., Fisher, B.E., Andrews, S.F., Lederhofer, J., Yap, C., Hatch, L., Stephens, T., Tsybovsky, Y., Crank, M.C., et al. (2021). A comprehensive influenza reporter virus panel for high-throughput deep profiling of neutralizing antibodies. Nat. Commun. 12, 1722. https:// doi.org/10.1038/s41467-021-21954-2.
- Mastronarde, D.N. (2005). Automated electron microscope tomography using robust prediction of specimen movements. J. Struct. Biol. 152, 36–51. https://doi.org/10.1016/j.jsb.2005.07.007.
- Punjani, A., Rubinstein, J.L., Fleet, D.J., and Brubaker, M.A. (2017). cryo-SPARC: algorithms for rapid unsupervised cryo-EM structure determination. Nat. Methods 14, 290–296. https://doi.org/10.1038/nmeth.4169.
- Rubinstein, J.L., and Brubaker, M.A. (2015). Alignment of cryo-EM movies of individual particles by optimization of image translations. J. Struct. Biol. 192, 188–195. https://doi.org/10.1016/j.jsb.2015.08.007.
- Sanchez-Garcia, R., Gomez-Blanco, J., Cuervo, A., Carazo, J.M., Sorzano, C.O.S., and Vargas, J. (2021). DeepEMhancer: a deep learning solution for cryo-EM volume post-processing. Commun. Biol. 4, 874. https://doi.org/10.1038/s42003-021-02399-1.
- Abramson, J., Adler, J., Dunger, J., Evans, R., Green, T., Pritzel, A., Ronneberger, O., Willmore, L., Ballard, A.J., and Bambrick, J. (2024). Accurate structure prediction of biomolecular interactions with AlphaFold. Nature 630, 493–500. https://doi.org/10.1038/s41586-024-07487-w.
- Pettersen, E.F., Goddard, T.D., Huang, C.C., Meng, E.C., Couch, G.S., Croll, T.I., Morris, J.H., and Ferrin, T.E. (2021). UCSF ChimeraX: Structure

- visualization for researchers, educators, and developers. Protein Sci. 30, 70-82. https://doi.org/10.1002/pro.3943.
- Adams, P.D., Grosse-Kunstleve, R.W., Hung, L.W., Ioerger, T.R., McCoy, A.J., Moriarty, N.W., Read, R.J., Sacchettini, J.C., Sauter, N.K., and Terwilliger, T.C. (2002). PHENIX: building new software for automated crystallographic structure determination. Acta Crystallogr. D Biol. Crystallogr. 58, 1948–1954. https://doi.org/10.1107/s0907444902016657.
- Emsley, P., and Cowtan, K. (2004). Coot: model-building tools for molecular graphics. Acta Crystallogr. D Biol. Crystallogr. 60, 2126–2132. https://doi.org/10.1107/S0907444904019158.
- Croll, T.I. (2018). ISOLDE: a physically realistic environment for model building into low-resolution electron-density maps. Acta Crystallogr. D Struct. Biol. 74, 519–530. https://doi.org/10.1107/S2059798318002425.
- 68. Georgiev, I.S., Joyce, M.G., Yang, Y., Sastry, M., Zhang, B., Baxa, U., Chen, R.E., Druz, A., Lees, C.R., Narpala, S., et al. (2015). Single-Chain Soluble BG505.SOSIP gp140 Trimers as Structural and Antigenic Mimics of Mature Closed HIV-1 Env. J. Virol. 89, 5318–5329. https://doi.org/10.1128/JVI.03451-14.
- Abu-Shmais, A.A., Vukovich, M.J., Wasdin, P.T., Suresh, Y.P., Marinov, T.M., Rush, S.A., Gillespie, R.A., Sankhala, R.S., Choe, M., Joyce, M.G., et al. (2024). Antibody sequence determinants of viral antigen specificity. mBio 15, e01560–01524. https://doi.org/10.1128/mbio.01560-24.
- Rush, S.A., Brar, G., Hsieh, C.L., Chautard, E., Rainho-Tomko, J.N., Slade, C.D., Bricault, C.A., Kume, A., Kearns, J., Groppo, R., et al. (2022). Characterization of prefusion-F-specific antibodies elicited by natural infection with human metapneumovirus. Cell Rep. 40, 111399. https://doi.org/10.1016/j.celrep.2022.111399.
- McLellan, J.S., Fau, C.M., Leung, S., Fau, L.S., Graepel, K.W., Yang, Y., Zhou, T., Baxa, U., Yasuda, E., et al. (2013). Structure of RSV fusion glycoprotein trimer bound to a prefusion-specific neutralizing antibody. Science 340, 1113–1117. https://doi.org/10.1126/science.1234914.
- Zhu, Q., McLellan, J.S., Kallewaard, N.L., Ulbrandt, N.D., Palaszynski, S., Zhang, J., Moldt, B., Khan, A., Svabek, C., McAuliffe, J.M., et al. (2017). A highly potent extended half-life antibody as a potential RSV vaccine surrogate for all infants. Sci. Transl. Med. 9, eaaj1928. https://doi.org/10. 1126/scitranslmed.aaj1928.
- Leuthold, M.M., Koromyslova, A.D., Singh, B.K., and Hansman, G.S. (2016). Production of Human Norovirus Protruding Domains in E. coli for X-ray Crystallography. J. Vis. Exp. e53845. https://doi.org/10.3791/53845.





STAR*METHODS

KEY RESOURCES TABLE

REAGENT or RESOURCE	SOURCE	IDENTIFIER
Antibodies		
Goat anti-human IgG-HRP	Thermo Fisher	Cat # A18817; RRID: AB_2535594
Mouse anti-RSV F (MCA490)	Bio-Rad	Cat# MCA490; RRID:AB_2231368
S309	PMID: 32422645	PBD: 6WS6
VRC01	BEI Resources	ARP-12033; RRID: AB_2491019
CR9114	PMID: 22878502	GenBank: JX213639, JX213640
MEDI8852	PMID: 27453466	RRID: AB_3111586
5-1	Abu-Shmais et al. ³⁵	N/A
APC-Cy7 Mouse Anti-Human CD14	BD	Cat# 561709; RRID: AB_10893806
FITC Anti-Human CD3 (OKT3)	Tonbo Biosciences	Cat# 35-0037; RRID: AB_2621662
BV711 Mouse Anti-Human CD19	BD	Cat# 563036; RRID: AB_2737968
PE-Cy5 Mouse Anti-Human IgG	BD	Cat# 551497; RRID: AB_394220
Bacterial and virus strains		
RSV A2 strain	BEI Resources	NR-52018
SARS-CoV-2 index pseudovirus	Daniel Sheward	N/A
SARS-CoV-1 pseudovirus	Daniel Sheward	N/A
SARS-CoV-2 Delta pseudotyped lentivirus	Daniel Sheward	N/A
SARS-CoV-2 Gamma pseudotyped lentivirus	Daniel Sheward	N/A
SARS-CoV-2 BA.2.75.2 pseudotyped lentivirus	Daniel Sheward	N/A
SARS-CoV-2 B.1 pseudotyped lentivirus	Daniel Sheward	N/A
SARS-CoV-2 BJ.1 pseudotyped lentivirus	Daniel Sheward	N/A
SARS-CoV-2 BA.2 pseudotyped lentivirus	Daniel Sheward	N/A
SARS-CoV-2 BA.5 pseudotyped lentivirus	Daniel Sheward	N/A
SARS-CoV-2 BQ.1.1 pseudotyped lentivirus	Daniel Sheward	N/A
SARS-CoV-2 JN.1 pseudotyped lentivirus	Daniel Sheward	N/A
SARS-CoV-2 XBB.1.5 pseudotyped lentivirus	Daniel Sheward	N/A
H5N1 A/Texas/37/2024	Rebecca A. Gillespie	N/A
H5N1 A/Vietnam/1203/2004	Rebecca A. Gillespie	N/A
H1N1 A/Michigan/45/2015	Rebecca A. Gillespie	N/A
H5N1 A/Cambodia/2023	Rebecca A. Gillespie	N/A
H5N2 A/Mexico/2024	Rebecca A. Gillespie	N/A
H2N2 A/Singapore/1/57	Rebecca A. Gillespie	N/A
Biological samples		
Human PBMCs (healthy)	StemCell Technologies	Cat# 70025
Human PBMCs (HIV-1+)	Mark Connors	N/A
Human PBMCs (COVID-19 convalescent)	Helen Chu	N/A
Human PBMCs (Influenza vaccinated)	Ted Ross	N/A
Chemicals, peptides, and recombinant proteins		
Polyethyleniminine Linear MW 25000	Polysciences	Cat#23966-1
1-Step Ultra TMB-ELISA Substrate Solution	Thermo Fisher	Cat#34029
Pluronic Acid F-68	Fisher	Cat# 24040-032
Bovine serum albumin (BSA)	Sigma-Aldrich	A1470
Ghost dye red 780	Tonbo biosciences	Cat#13-0865
4 841 1 1 1 1	Fisher	Cat# 25030-081
4 mM L-glutamine Protein A resin	GenScript	Cat#L00210

(Continued on next page)





Continued		
REAGENT or RESOURCE	SOURCE	IDENTIFIER
Lyra-CoV Spike	Wall et al. ³¹	N/A
SARS-CoV-2 Index RBD	Sino Biological	Cat# 40592-VNAH
SARS-CoV-2 HexaPro Index Spike	PMID: 32703906	N/A
SARS-CoV-1 S	Jason McLellan	N/A
HCoV-OC43 S	Jason McLellan	N/A
HCoV-HKU1-S-2P	PMID: 28807998	N/A
RSV A2 DS-Cav1 prefusion F	Jason McLellan	N/A
RSV B9320 DS-Cav1 prefusion F	Jason McLellan	N/A
RSV post-fusion	Jason McLellan	N/A
hMPV F A1(NL/1/00)	Jason McLellan	N/A
hMPV F B2(TN99-419)	Jason McLellan	N/A
hMPV A postfusion F	Jason McLellan	N/A
Parainfluenza virus type 3 prefusion stabilized F ectodomain	PMID: 30420505	PDB: 6MJZ
H5/TX/24 hemagglutinin	Genscript	GenBank PP577943.1
H3 HK68	Masaru Kanekiyo	N/A
H3 Perth19	Masaru Kanekiyo	N/A
H1 MI15	Masaru Kanekiyo	N/A
H1 NC99	Masaru Kanekiyo	N/A
B2 SG57	Masaru Kanekiyo	N/A
HA B/Wash/19	Masaru Kanekiyo	N/A
H5 VN04	Masaru Kanekiyo	N/A
H5 IN05	Masaru Kanekiyo	N/A
H7 Anh13	Masaru Kanekiyo	N/A
H5 HK09	Masaru Kanekiyo	N/A
H10 JD13	Masaru Kanekiyo	N/A
HIV-1 gp140 SOSIP BG505	Ivelin Georgiev	N/A
HIV-1 ZM197 env	Ivelin Georgiev	N/A
HIV-1 B4.1 env	Ivelin Georgiev	N/A
Norovirus CHDC P domain	Grant Hansman	N/A
Norovirus SYD_2012 P domain	Grant Hansman	N/A
Norovirus GII.17 P domain	Grant Hansman	N/A
Critical commercial assays		
B cell Single Cell V(D)J solution	10X Genomics	N/A
ExpiFectamine™ 293 Transfection Kit	Thermo Fisher	Cat #A14526
EZ-link Sulfo-NHS-Biotin No-Weigh	Thermo Fisher	Cat #A39258
Solulink protein-oligonucleotide conjugation kit	TriLink Biotechnologies	Cat#S-9011
Plasmid Kits for Plasmid DNA Extraction	QIAGEN	Cat#12165
StrepTrap XT prepacked chromatography column	Cytiva	Cat#29401322
Deposited data		
Raw next-generation sequencing data	This paper	SRA: PRJNA1321287
Cryo-EM structure RSV-3301 and RSV-2245 fabs bound to RSV-A F	This paper	PDB: 9MKN, EMDB: EMD-48331
Experimental models: Cell lines		
Human: Expi293F cells	Thermo Fisher	Cat#A14527
HEK293T	ATCC	CRL-3216
Vero cells	ATCC	CCL-81
E. coli DH5α	Cell Culture Core	N/A
L. 00,1 DI 100	Jon Juliuro Jore	1 1// 1

(Continued on next page)





Continued		
REAGENT or RESOURCE	SOURCE	IDENTIFIER
Oligonucleotides		
Oligonucleotides for protein DNA-barcoding	Setliff et al. ¹⁹	N/A
Software and algorithms		
Cell Ranger	10X Genomics	https://support.10xgenomics.com/single-cell-gene-expression/software/downloads/latest
HighV-Quest	Brochet et al. ⁵⁰	https://www.imgt.org/HighV-QUEST/.
GraphPad Prism 9.5.0	https://www.graphpad.com/	N/A
Octet Data Analysis Software v11.1	N/A	N/A
cryoSPARC v4.6.0	N/A	N/A
DeepEMhancer	N/A	N/A
AlphaFold 3	N/A	N/A
Phenix v1.21.2	N/A	N/A
Coot v0.9.2	N/A	N/A
ISOLDE v1.8	N/A	N/A
GraphPad Prism v10.1.0	https://www.graphpad.com/	N/A
ANARCI	N/A	N/A
BioPhi OASis	N/A	N/A
SignalP v6.0	N/A	N/A
Flowjo v10	TreeStar	https://www.flowjo.com/
Other		
Python scripts for antibody generation and analysis	This paper	https://github.com/IGlab-VUMC/MAGE_ab_ generation
Finetuned model weights	This paper	https://huggingface.co/perrywasdin/MAGE_V1

EXPERIMENTAL MODEL AND STUDY PARTICIPANT DETAILS

Cell lines used in this study include Expi293F (Thermo Fisher), HEK293T (ATCC), and Vero cells (ATCC). Bacterial strains used include E. coli DH5 α (Thermo Fisher). Cells were maintained at 37 $^{\circ}$ C and authenticated by the vendors. All cells were regularly tested for mycoplasma contamination and confirmed negative.

METHOD DETAILS

MAGE model development

Database curation

The training database used to finetune MAGE for antibody generation consisted of paired human antibody sequences with cognate antigen sequences curated based on known antigen specificities. These sequence pairs were curated from public databases and literature, primarily the CoV-AbDab, PIAbDab, and SabDab. 8-10 For the PIAbDab, due to vague antigen labels (e.g. "flu"), sequences were manually curated from referenced literature. 11,15-18,51,52 Sequences were also sources from previously published LIBRA-seq datasets 19,20,22,23 and other recent literature. 14,21 For all training sequences, heavy and light chains less than 100 amino acid residues in length were removed. When not provided by sources, antigens sequences were obtained from Uniprot. 53 For all antigen sequences, signal peptides were removed using SignalP 6.0. 54 See provided Python scripts and Table S1 for further details on filtering and thresholds applied for individual data sources, along with counts for antigen-specificities and sources included in training.

Fine-tuning

The pretrained general protein model Progen2-base was fine-tuned for the task of generating paired heavy and light chain antibody sequences in response to an antigen prompt. This was achieved by autoregressive finetuning of Progen2-base's 764 million parameters on sequences consisting of paired heavy and light chain antibodies and their cognate antigens. For each training example, these sequences were input to the model as a single concatenated vector with separation tokens between each sequence:

<|bos> [Input antigen sequence] | SEP] [heavy chain sequence] | LC] [light chain sequence] <| eos|>

with two new special tokens, '[SEP]' and '[LC]' added to the Progen2 tokenizer. The training loss dropped rapidly in less than a single epoch (Figure S1C), demonstrating the ability of the pretrained model to quickly adapt to the new task and prompt format. During training, 10% of the data was held-out for evaluation during training to monitor overfitting and generalization. Fine-tuning





was performed using HuggingFace⁵⁵ Trainer for causal language modeling, with the Adam optimizer. The loss function was modified to mask the antigen sequence so that the mean negative loglikelihood loss was calculated across the antibody sequence only during training (excluding the antigen sequence and [SEP]). Loss was calculated after each step in training, while evaluation loss and accuracy were calculated every 500 steps using the evaluation data, for a total of 5 epochs (10,415 training steps). A learning rate of 1x10⁻⁵ was used with the default linear learning rate scheduler in HuggingFace. A training batch size of 8 was used, distributed across 4 Tesla V100 GPUs.

Antibody generation and basic filtering

Based on the minimum evaluation loss, antibodies were generated using the model checkpoint saved after epoch 4. For generation of antibodies against an antigen target, the fine-tuned model was prompted with the entire antigen amino acid sequence using a probability threshold of 0.9 and a temperature of 1. The maximum sequence length was limited to the length of the input antigen sequence plus 250, allowing for a total length of 250 for the combined heavy and light chain. This length limit was not necessary for the model to generate quality antibody sequences, as multiple pad tokens were always generated following the end of the light chain sequence. In alignment with the format of the training data, the generated sequences were in the format:

<|bos> [Input antigen sequence] [SEP] [heavy chain sequence] [LC] [light chain sequence] <|pad|>n. <|eos|>

In order to separate out the generated antibody chains without introducing bias, the chains were simply selecting by splitting the string at the '[SEP]' and '[LC]' tokens, then truncating the light chain at the appearance of the first pad token (<|pad|>). Since the maximum length allowed for generation was 250 residues, most sequences contained extra pad tokens at the end of the sequences following the light chain, which were removed.

Following selection of the generated heavy and light variable regions, the antibody sequences were annotated using ANARCI⁵⁶ with IMGT²⁴ numbering. If a sequence had either a heavy or light chain that was not recognized as a human variable chain by ANARCI, it was discarded, along with any sequences missing framework or CDR regions following alignment. Heavy chains or light chains shorter than 100 amino acids were also discarded, although few sequences under these lengths survived the previous filtering steps. Heavy chains which were identical to a training example were discarded, although there was only one occurrence of this in the sequences generated against SARS-CoV-2 RBD. Finally, antibodies were assessed for mutational load based on identity to germline variable genes, and humanness using the BioPhi OASis software.

Perplexity was calculated by performing a backward pass through the trained model, with the model in evaluation mode, to calculate the exponential of the average negative log-likelihood for each generated sequence.

Antibody selection for experimental validation

For antibodies generated by prompting with SARS-CoV-2 RBD, additional criteria were applied to select candidates for experimental validation. For the heavy variable gene, only sequences with >85% identity were retained. For humanness, sequences below 70th percentile were discarded based on the recommended threshold for OASis. 25 In order to test novel sequences generated by the model, antibodies with a CDRH3 identical to any training example (n = 72), or a VH germline identity of 100% (n = 175) were removed, leaving a selection pool of 732 antibodies. In addition, any sequences with both >90% VH identity and >90% CDRH3 identity to CoV-AbDab RBD binding antibody sequences were removed. Following these filtering steps, the following automated selected pipeline was applied:

- From the top 5 most frequently generated VH genes, select sequences with 20th and 80th percentile VH identities.
- Select top 5 sequences by rank of maximum CDRH3 identity to known binding antibodies.
- Select top 5 sequences by rank of maximum VH identity to know binding antibodies.

Together, these three selection steps yield 20 antibodies per antigen target. Antibodies from Step 1 represent selection independent of known binding antibodies to avoid any bias, while antibodies from Steps 2 and 3 yield testing antibodies with high similarity to known binding antibodies.

For RSV-specific candidates, MAGE was prompted using the RSV-A Fusion glycoprotein F0 (UniProt⁵³ entry P03420) amino acid sequence to generate 10,000 sequences for down selection and validation. Basic filtering was applied as described above, along with filtering based on perplexity (PPL < 1.5), heavy chain germline identity (percent VH identity < 98%), and sequence identity to training antibodies (maximum CDRH3 identity to any training antibody ≤ 95%). Due to the overrepresentation of CoV-specific antibodies seen in training, the remaining generated sequences were compared to CoV-AbDab antibodies to remove sequences with CDRH3s similar to CoV-specific antibodies (CDRH3 percent identity > 70%).

Following filtering, antibodies were selected for validation based on three separate criteria groups. First, an unbiased group was selected by clustering generated CDRH3s using hierarchical clustering based on a Levenshtein identity matrix with a maximum identity distance of 20% within each cluster. One sequence was then randomly sampled from each of the top 10 largest clusters, for a total of 10 unbiased sequences selected for validation. For the unbiased group, we selected generated sequences with CDRH3 identity ≥75% and equal CDRH3 length compared RSV-A-specific training antibodies. From these matches, 10 antibodies were randomly selected from unique CDRH3 clusters. Finally, three generated antibodies with CDRH3 identity >70% to RSV-A-specific training antibodies and CDRH3 identity ≥60% to MPV-A-specific training antibodies were selected. In total, 23 antibodies were selected for experimental validation.

For H5N1-specific candidates, MAGE was prompted using the highly pathogenic avian influenza virus H5/TX/24 hemagglutinin sequence (Strain A/Texas/37/2024, GenBank accession number PP577943.132) amino acid sequence as a prompt to generate





1,000 sequences for down selection and validation. Basic filtering was applied as described above, along with filtering based on heavy chain germline identity (percent VH identity < 100%). Antibodies were then selected for validation based on CDRH3 Levenshtein identity to H5-specific training antibodies. Generated sequences were randomly selected from four CDRH3 identity bins: [80% - 85%) (n = 3), [85% - 90%) (n = 6), [90% - 95%) (n = 6), and [95% - 99%) (n = 3) for a total of 18 antibodies. Since this exact flu strain sequence was not seen in training, no unbiased group was selected for testing.

Training consensus sequence alignments

Developability profiles with Therapeutic Antibody Profiler (TAP)

The following consensus alignment was performed for each antigen target presented. Training antibodies for comparison were selected based on antigen sequence identity using thresholds of 0.95 for RBD (to capture only index strain-specific antibodies), 0.9 for H5, and 0.9 for RSV-A F. Within these groups, antibodies were grouped by VH gene and numbered with the IMGT numbering scheme using ANARCI. For residues in the VH region up to, but excluding, the CDRH3, a consensus sequence was constructed by finding the most frequently used amino acid at each position. MAGE-generated antibodies were then compared to these consensus sequences, grouped based on antigen-specificity and VH gene usage, using Levenshtein distance of the VH region.

For experimentally validated antibodies, the sequences were analyzed using the TAP2 web server to compare antibody variable chain sequences to the clinical stage therapeutic guidelines. For each metric, the values for all clinical-stage antibodies presented in Raybould et al. were obtained from the provided supplemental data and visualized for comparison to the MAGE-generated antibodies.

Antibody candidate validation Antibody expression and purification

For validation and characterization of generated antibody sequences, variable genes were synthesized as cDNA and were inserted into bi-cistronic plasmids encoding for the constant regions of the heavy chain and either the kappa or lambda light chain, for each antibody (Twist BioScience). DH5 α cells were transformed with the antibody DNA, and the resulting ampicillin resistant colonies were grown in LB broth. Plasmid DNA was isolated from the bacterial cultures using a plasmid purification kit (Qiagen). The purified antibody DNA was transfected into Expi293F cells using ExpiFectamine transfection reagent (Thermo-Fisher Scientific), and antibodies transiently expressed in FreeStyle F17 expression media (Thermo-Fisher) supplemented 0.1% Pluronic Acid F-68 and 20% 4 mM L-glutamine. Cells were cultured at 8% CO₂ saturation and 37°C with shaking. Cells were collected five days post transfection and centrifuged at a minimum of 5,000 rpm for 20 minutes. Filtered supernatant (Nalgene Rapid Flow Disposable Filter Units with PES membrane 0.45 or 0.22 μ m) was purified over protein A equilibrated with PBS. Antibodies were eluted from the column with 100 mM glycine HCl at pH 2.7 directly into a 1:10 volume of 1 M Tris-HCl pH 8 and then buffer exchanged into PBS for storage at 4°C. **Antigen expression and purification**

For the different binding experiments, SARS-CoV-2 Index S RBD (2019-nCoV) was purchased from Sino Biological catalog number (40592-VNAH) while SARS-CoV-2 S Hexapro Index strain, SARS-CoV-2 S XBB.1, and SARS-CoV-1 S were expressed in Expi293F cells by transient transfection in FreeStyle F17 expression media (Thermo-Fisher) supplemented to a final concentration of 0.1% Pluronic Acid F-68 and 20% 4 mM L-glutamine using ExpiFectamine transfection reagent (Thermo-Fisher) cultured for 4-7 days at 8% CO₂ saturation and 37°C with shaking. After transfection, cultures were centrifuged at 5000 rpm for 20 minutes. Filtered supernatant (Nalgene Rapid Flow Disposable Filter Units with PES membrane 0.45 or 0.22 μm), was run slowly over equilibrated, 1 mL pre-packed StrepTrap XT column (Cytiva Life Sciences). The column was washed with 15 mL of binding buffer (100 mM Tris-HCl, 150 mM NaCl, 1 mM EDTA, pH 8.0), and purified protein was eluted from the column with 10 mL of binding buffer supplemented with 2.5 mM desthiobiotin. Protein was concentrated, buffer exchanged into PBS and run on a Superose 6 Increase 10/300 GL on the AKTA FPLC system. Peaks corresponding to trimeric species were identified based on elution volume and SDS-PAGE of elution fractions. Fractions containing pure spike were pooled.

Lyra-CoV Spike and BG505 SOSIP v9.3 were expressed in Expi293F cells via transient transfection using ExpiFectamine (Thermo Fisher) in FreeStyle F17 media (Thermo Fisher) supplemented with 0.1% Pluronic F-68 and 4 mM L-glutamine. Cultures were incubated at 37° C with 8% CO₂ and shaking for 5–7 days, then centrifuged at 4,000 rpm for 20 minutes. Supernatants were filtered through 0.45 or 0.22 μ m PES membranes (Nalgene Rapid-Flow).

Filtered supernatant was loaded onto a 1 mL HisTrap HP column (Cytiva) pre-equilibrated with wash buffer (20 mM sodium phosphate, 0.5 M NaCl, 20 mM imidazole, pH 7.4). After washing with 15 mL of the same buffer, bound protein was eluted with 15 mL of elution buffer (20 mM sodium phosphate, 0.5 M NaCl, 500 mM imidazole, pH 7.4). Eluted protein was concentrated, buffer exchanged into PBS, and further purified by size-exclusion chromatography on a Superose 6 Increase 10/300 GL column using an ÄKTA FPLC system. Trimeric species were identified by elution volume and SDS-PAGE, and pure fractions were pooled.

Enzyme-linked immunosorbent assay (ELISA)

Recombinant antigen (SARS-CoV-2 Index RBD, SARS-CoV-2 Index S, XBB.1 spike, SARS-CoV-1 S) was plated at 2 μ g/mL overnight at 4°C. The next day, plates were washed three times with PBS supplemented with 0.05% Tween20 (PBS-T) and coated with 5% bovine serum albumin (BSA) in PBS-T. Following a one-hour incubation at room temperature (RT), the plates were washed three times with PBS-T. Primary antibodies diluted in 1% BSA in PBS-T were then added to the plates, starting at 10 μ g/mL with a serial 1:5 dilution, followed by a one-hour incubation at RT. Plates were then washed three times in PBS-T before adding secondary antibody, goat anti-human IgG conjugated to peroxidase, at 1:10,000 dilution in 1% BSA in PBS-T followed by a one-hour incubation at RT. Plates were washed for a final three times with PBS-T and then developed by adding TMB substrate to each well. Plates were





incubated at RT for five minutes, and then 1 N sulfuric acid was added to stop the reaction. Plates were read at 450 nm. ELISAs were performed in technical and biological duplicate. The area under the curve (AUC) values were calculated using GraphPad Prism 9.5.0 to fit a 4-parameter log(agonist) vs. response curve.

Biolayer interferometry

BLI experiments were performed using an OctetRED96e instrument (Sartorius) at 21°C and a shaking speed of 1000 rpm. For the RBD-binding antibodies, purified SARS-CoV-2 Wuhan- Hu-1 RBD-SD1 (residues 319–591) containing a C-terminal 8xHis tag was immobilized to Ni-NTA sensortips (Sartorius) to a response level of approximately 1.5 nm in HBS-P buffer (10 mM HEPES pH 7.4, 150 mM NaCl, 0.005% v/v Surfactant P20) with 20 mM imidazole and 0.1% w/v BSA added. After a 60 s baseline step, immobilized RBD-SD1 was dipped into wells containing 2-fold serial dilutions of IgG ranging in concentration from 32 to 0.5 nM (RBD-159, RBD-238, RBD-409, RBD-839, and RBD-951) or 1024–16 nM (RBD-446) to measure association. 1.5-fold dilutions ranging from 1024 to 90 nM of RBD-61 and a combination of 1.5-fold (1024–303 nM) and 2-fold (303–38 nM) dilutions of RBD-413 were used to optimize the dynamic range of the binding curves for those antibodies. Dissociation was measured by dipping sensortips into wells containing buffer only. Data were reference subtracted and kinetics were calculated (high-affinity antibodies only) by fitting curves to a 1:2 bivalent analyte model using the Octet Data Analysis Software v11.1.

Binding specificity was measured by immobilizing 8xHis-tagged SARS-CoV-2 Wuhan-Hu-1 RBD-SD1 or 8xHis-tagged prefusion-stabilized RSV F trimer (DS-Cav1²⁸) to Ni-NTA sensortips to a response level of approximately 1.5 nm in the buffer described above. Immobilized antigen was then dipped into wells containing the anti-RBD IgG of interest (4, 16, or 512 nM antibody for immobilized RBD-SD1 and 512 nM antibody for immobilized RSV F). Immobilized RSV F was also dipped into wells containing only buffer to observe baseline signal drift.

For the RSV F-binding antibodies (Figure S5), purified 8xHis-tagged prefusion-stabilized RSV F trimer (DS-Cav1) was immobilized to Ni-NTA sensortips to a response level of approximately 0.8 nm in HBS-P buffer with 20 mM imidazole and 0.1% w/v BSA added. After a 60 s baseline step, immobilized Ds-Cav1 was dipped into wells containing 2-fold serial dilutions of Fab ranging in concentration from 640 to 10 nM (RSV-2245) or 5 to 0.78 μ M (RSV-3301) to measure association. Dissociation was measured by dipping sensortips into wells containing buffer only. Data were reference subtracted and kinetics were calculated by fitting curves to a 1:1 (RSV-2245) or heterogeneous ligand (RSV- 3301) model using the Octet Data Analysis Software v11.1.

SARS-CoV-2 Pseudovirus Neutralization Assay

Pseudovirus neutralization assays were performed as previously described.⁵⁷ Briefly, spike-pseudotyped lentiviruses were produced by the co-transfection of HEK293T cells with respective spike variant plasmids, together with an HIV gag-pol packaging plasmid (Addgene #8455) and a firefly luciferase encoding transfer plasmid (Addgene #170674). Transfections were performed using polyethylenimine. Pseudoviruses titrated to produce approximately 100,000 RLU were incubated with 8 serial 3-fold dilutions for 1 hour at 37°C in black-walled 96-well plates. 10,000 HEK293T-ACE2 cells were then added to each well, and plates were incubated at 37°C. Luminescence was measured approximately 48 hours later on a GloMax Navigator Luminometer (Promega) using Bright-Glo luciferase substrate (Promega) as per the manufacturer's recommendations. Neutralization was calculated relative to the average of 8 control wells infected in the absence of antibody. IC₅₀ values were calculated by fitting a four-parameter logistic curve and interpolating the concentration at which there is 50% neutralization, using GraphPad Prism v10.1.0.

RSV Neutralization Assay

RSV neutralization assays were performed similarly to previously described protocols (PMID: 37403896). In brief, Vero cells were seeded the day before the assay at a density of 2x10⁴ cells per well in a 96-well plate in high glucose DMEM supplemented with L-glutamine and 10% FBS. Monoclonal antibodies were 2-fold serially diluted starting from a concentration of 50 μg/mL in DMEM supplemented with 2% FBS and each antibody dilution was mixed with an equal volume of the same medium containing 100 TCID50 of RSV virus strain A2 (cat n. NR-52018, BEI Resources) and incubated for 1 hour at 37°C, 5% CO₂. Uninfected and infected cell wells without the antibody were also included as controls. After the incubation, the antibody-virus mixtures were added to the cells and plates were incubated at 37°C, 5% CO₂ for 72 hours. Plates were then washed with PBS and cells fixed with cold 80% v/v acetone in PBS for 10 minutes at RT. After the incubation, the plates were emptied and washed 3 times with wash buffer (PBS + 0.3% Tween20). Primary mouse anti-RSV F antibody (cat n. MCA490, Bio-Rad) diluted at 1:1,000 in blocking buffer (wash buffer + 7.5% BSA) was then added to the plates and incubated for 1 hour at RT. Following the incubation, the plates were washed 3 times with wash buffer and secondary goat anti-mouse IgG human adsorbed HRP-conjugated secondary antibody (cat. n. 1030-05, Southern Biotech) diluted 1:1,000 was added and incubated for 1 hour in the dark at RT. Plates were then washed 5 times with wash buffer and freshly prepared o-Phenylenediamine dihydrochloride (OPD) substrate added and incubated for 3-5 minutes at RT. Reaction was stopped by adding 2N H₂SO₄ and absorbance read at 490 nm using a PowerWaveXS plate reader (BioTek).

Influenza reporter virus neutralization assay

Generation of the replication-restricted reporter (R3 Δ PB1) H1N1 virus (A/Michigan/45/2015) as well as rewired R3 Δ PB1 (R4 Δ PB1) H5N1 virus (A/Vietnam/1203/2004) is described elsewhere. R4 Δ PB1 H5N1 A/Texas/37/2024 virus was prepared similarly. Briefly, to generate the R3/R4 Δ PB1 viruses the viral genomic RNA encoding functional PB1 was replaced with a gene encoding the fluorescent protein (TdKatushka2), and the R3/R4 Δ PB1 viruses were rescued by reverse genetics and propagated in the complementary cell line which expresses PB1 constitutively. Each R3/R4 Δ PB1 virus stock was titrated by determining the fluorescent units per mL (FU ml $^{-1}$) prior to use in the experiments. For virus titration, serial dilutions of virus stock in OptiMEM were mixed with pre-washed MDCK-SIAT1-PB1 cells (8 \times 10 5 cells/ml) and incubated in a 384-well plate in quadruplicate (25 μ l well $^{-1}$). Plates were incubated





for 18–26 h at 37°C with 5% CO $_2$ humidified atmosphere. After incubation, fluorescent cells were counted by using a Celigo Image Cytometer (Nexcelom) with a customized red filter for detecting TdKatushka2. For the microneutralization assay, serially diluted antibodies were prepared in OptiMEM and mixed with an equal volume of R3/R4 Δ PB1 virus (\sim 8 × 10^4 FU ml $^{-1}$) in OptiMEM. After incubation at 37°C and 5% CO $_2$ humidified atmosphere for 1 h, pre-washed MDCK-SIAT1-PB1 cells (8 × 10^5 cells well $^{-1}$) were added to the antibody-virus mixtures and transferred to 384-well plates in quadruplicate (25 μ l well $^{-1}$). Plates were incubated and counted as described above. Target virus control range for this assay is 500 to 2,000 FU per well, and cell-only control is acceptable up to 30 FU per well. The percent neutralization was calculated for each well by constraining the virus control (virus plus cells) as 0% neutralization and the cell-only control (no virus) as 100% neutralization. A 7-point neutralization curve was plotted against antibody concentration for each sample, and a four-parameter nonlinear fit was generated using Prism (GraphPad) to calculate the 50% (IC $_{50}$) inhibitory concentrations.

Cryo-EM sample prep and data collection

RSV F (prefusion-stabilized, PR-DM 36 was mixed to a final concentration of 2.5 mg/mL with 1.5X molar excess of Fabs RSV-2245 and RSV-3301 in buffer containing 2 mM Tris pH 7.5, 200 mM NaCl, 0.02% NaN $_3$. The complex was incubated for 30 minutes at 4 °C before adding 10X CMC CHAPS (VitroEase $^{\text{TM}}$ Buffer Screening Kit, Thermo Fisher) to a final concentration of 0.1X CMC. Immediately following the addition of CHAPS, 3.5 μ L of sample was applied to C-flat 1.2/1.3 300 mesh grids (Electron Microscopy Sciences) that had been glow discharged using a PELCO easiGlow (Ted Pella) for 30 s at a current of 20 mA. Using a Vitrobot Mark IV (Thermo Fisher), a blot force of 1 was applied for 9 s to blot away excess liquid before plunge-freezing into liquid ethane. Samples were blotted in 100% humidity at 4 °C.

1,561 movies were collected from a single grid using a Glacios TEM (Thermo Fisher) equipped with a Falcon 4 detector (Thermo Fisher), with the stage tilted to 30°. All movies were collected using SerialEM v4.0.10 automation software. ⁵⁹ Particles were imaged at a calibrated magnification of 0.933 Å/pixel, with an exposure of 2.5 eps for 17s for a total exposure of 49 e/Å2. Additional details about data collection parameters can be found in Table S3.

Cryo-EM processing and structure building

Motion correction, CTF estimation, particle picking, and preliminary 2D classification were performed using cryoSPARC v4.6.0 live processing ⁶⁰ (Figure S7). An initial ab initio reconstruction of four classes was performed during live processing using 123,151 particles. Once data collection was completed, a final iteration of 2D class averaging distributed 610,184 particles into 80 classes using an uncertainty factor of 1 and a batchsize of 300 for 25 iterations. From that, 338,721 particles were selected and carried into a heterogeneous refinement of the four volumes that resulted from the initial ab initio reconstruction. Particles from the highest quality class were used for homogenous refinement of the best volume with applied C3 symmetry. To address remaining particle heterogeneity, 210,844 particles (after re-extraction and duplicate removal) were sorted into four classes by performing another Ab initio reconstruction, followed by heterogeneous refinement of the four classes using all particles. From this, 140,634 particles were taken from the best class and used for a final non-uniform refinement with applied C3 symmetry and with refined per-particle defocus and per-group CTF parameters. To improve map quality, the refinement volumes were processed using DeepEMhancer within cryoSPARC. An initial model of the complex was generated using AlphaFold 3 (https://alphafoldserver.com) by inputting sequences (separately) for RSV F1 and F2, 2245 VH and VL, and 3301 VH and VL. The highest confidence output model was docked into the refined volume via ChimeraX v1.8. The structure was iteratively refined and completed using a combination of Phenix v1.21.2, 65 Coot v0.9.2, 66 and ISOLDE v1.8.

LIBRA-seq Experiments

LIBRA-seq antigen expression

For the LIBRA-seq antigen panel, a total of 29 proteins were expressed as recombinant soluble antigens. Influenza, parainfluenza, coronavirus, RSV post fusion, hMPV post fusion, and HIV-1 antigens were expressed as described above and then purified over the appropriate affinity column at 4°C.

Recombinant hemagglutinin (HA) proteins all contained the HA ectodomain with a point mutation at the sialic acid-binding site (Y98F), a T4 fibritin foldon trimerization domain, and a hexahistidine-tag. HAs were purified by metal affinity chromatography. Parainfluenza virus type 3 prefusion stabilized F ectodomain (PDB: 6MJZ) was purified by nickel affinity chromatography. SARS-CoV-2 S XBB.1, BQ.1.1, SARS-CoV-1 S, HCoV-OC43 S, HCoV-HKU1-S-2P, RSV post fusion, and hMPV post fusion were purified over pre-packed StrepTrap XT column (Cytiva Life Sciences), as described above. Single chain HIV-1 gp140 SOSIP variant strain BG505⁶⁸ was purified over agarose bound Galanthus nivalis lectin (Vector Laboratories cat no. AL-1243-5). Methods have been previously described.⁶⁹

Previously described hMPV F A1(NL/1/00) and B2(TN99-419) antigens were expressed in FreeStyle 293-F cells by transient transfection in FreeStyle 293 expression media (Thermo-Fisher). Cells were co-transfected at a 4:1 ratio of plasmids encoding human metapneumovirus F and furin, respectively, using polyethylenimine (PEI). Three hours post-transfection, media was supplemented to a final concentration of 0.1% (v/v) Pluronic Acid F-68. After culturing for 6 days at 37°C and 8% CO₂ saturation, filtered supernatant was concentrated and buffer exchanged to PBS using tangential flow filtration. Samples were then run over a gravity-flow affinity column at RT. Previously described RSV F (DS-Cav1) A2 and B9320 antigens were expressed similarly but did not include the Pluronic F-68 supplementation step. Stabilized ectodomains of hMPV F subtypes A1 and B2,⁷⁰ as well as RSV strains A2^{28,71} and B9320 F (DS-Cav1⁷²), were purified over Strep-Tactin Sepharose resin (IBA Lifesciences) in a gravity column.

CHDC, SYD_2012, and GII.17 P domains were recombinantly expressed and purified as previously described.⁷³





All proteins were quantified using UV/vis spectroscopy. Antigenicity of proteins was characterized by ELISA with known monoclonal antibodies specific for that antigen. Proteins were frozen and stored at -80°C until use. Protein antigens were biotinylated using EZ-link Sulfo-NHS-Biotin No-Weigh kit (Thermo Fisher) according to manufacturer's instructions. A 50:1 biotin-to-protein molar ratio was used for all reactions.

LIBRA-seq antigen barcodes

For each antigen, a unique DNA barcode was directly conjugated to the antigen using a SoluLINK Protein-Oligonucleotide Conjugation kit (TriLink, S-9011) according to manufacturer's protocol. We used oligonucleotides composed of a 15 bp antigen barcode, a sequence designed for annealing to the template switch oligo on the 10X bead-delivered oligos, and contains truncated TruSeq small RNA read 1 sequences in the following structure: 5'-CCTTGGCACCCGAGAATTCCANNNNNNNNNNNNNNNCCCATATAAGA*A*A-3', where Ns represent the antigen barcode. For each antigen we used the following barcode sequences:

Norovirus GII.4 Sydney P (ATTCGCCTTACGCAA), Norovirus CHDC P (AACCTTCCGTCTAAG), Norovirus GII.17 P (GCAGCGTATA AGTCA), HIV-1 env BG505 (TAACTCAGGGCCTAT), HIV-1 env B4.1 (TACGCCTATAACTTG), HIV-1 env ZM197 (CAGATGATCAC CAT), SARS-CoV-2 XBB.1 (AGACTAATAGCTGAC), SARS-CoV-2 BQ.1.1 (CTTCACTCTGTCAGG), SARS-1 (TGGTAACGACA GTCC), HCoV-OC43 (GACCTCATTGTGAAT), HCoV-HKU1 (CAGCCCACTGCAATA), H3 HK68 (AACCCACCGTTGTTA), H3 Perth19 (GACAAGTGATCTGCA), H1 MI15 (GCTCCTTTACACGTA), H1 NC99 (TGTGTATTCCCTTGT), H2 SG57 (GGTAGCCCTAGAGTA), HA B/Wash/19 (TGACCTTCCTCTCT), H5 VN04 (TCACAGTTCCTTGGA), H5 IN05 (TCATTTCCTCCGATT), H7 Anh13 (CAGTAGATGGA GCAT), H9 HK09 (CAGTAAGTTCGGGAC), H10 JD13 (CCGTCCTGATAGATG), RSV-A F (TTTCAACGCCCTTTC), RSV-B F (GTGTGT TGTCCTATG), RSV-A post fusion F (AATCACGGTCCTTGT), MPV-A F (CAGGTCCCTTATTTC), MPV-B F(ACAATTTGTCTGCGA), MPV-A post fusion F (ATCGTCGAGAGCTAG), PIV-3 F (GTAAGACGCCTATGC).

Oligos were ordered from Sigma-Aldrich and IDT with a 5' amino modification and HPLC purified.

Donor peripheral blood mononuclear cell (PBMCs) samples

Healthy peripheral blood mononuclear cell (PBMC) samples were purchased from StemCell Technologies. SARS-CoV-2 PBMCs were collected from individuals with SARS-CoV-2 infection, 60 days post symptom onset during May-June 2020. Influenza vaccination PBMCs were collected from individuals 28 days following vaccination with the 2021-2022 quadrivalent flu vaccine. HIV-1 PBMCS were collected between 2007-2013 from individuals with confirmed HIV-1 status.

Flow cytometry enrichment of antigen-specific B cells

For a given sample, cell mixtures were stained and mixed with fluorescently labeled DNA-barcoded antigens and other antibodies, and then sorted using fluorescence activated cell sorting (FACS). Cells were counted, washed with DPBS supplemented with 0.1% Bovine serum albumin (BSA), and resuspended in DPBS-BSA to be stained with the following cell markers: Ghost Red 780, CD14-APCCy7, CD3-FITC, CD19-BV711, and IgG-PECy5. Additionally, antigen-oligo conjugates were added to the stain. Following a 30-minute incubation in the dark on ice, the cells were washed three times with DPBS-BSA then incubated for 15 minutes in the dark on ice with Streptavidin-PE label cells with bound antigen. Cells were then resuspended in DPBS-BSA and sorted on the cell sorter. Antigen positive cells were bulk sorted and then delivered to the Vanderbilt VANTAGE sequencing core at an appropriate target concentration for 10X Genomics library preparation and subsequent sequencing. FACS data were analyzed using FlowJo.

Sequence processing and bioinformatics analysis for LIBRA-seq

We followed our established pipeline, ¹⁹ which takes paired-end FASTQ files of oligonucleotide libraries as input, to process and annotate reads for cell barcodes, unique molecular identifiers (UMIs) and antigen barcodes, resulting in a cell barcode-antigen barcode UMI count matrix. B cell receptor contigs were processed using CellRanger 3.1.0 (10x Genomics) and GRCh38 Human V(D)J 7.0.0 as reference, while the antigen barcode libraries were also processed using CellRanger (10x Genomics). The cell barcodes that overlapped between the two libraries formed the basis of the subsequent analysis. Cell barcodes that had only non-functional heavy chain sequences as well as cells with multiple functional heavy chain sequences and/or multiple functional light chain sequences, were eliminated, reasoning that these may be multiplets. We also aligned the B cell receptor contigs to IMGT reference genes using HighV-Quest. ⁵⁰ The annotated sequences were then combined with an antigen barcode UMI count matrix. Finally, we determined the LIBRA-seq score (LSS) for each antigen in the library for every cell as previously described. ¹⁹ Binding was defined using a conservative threshold of LSS \geq 2, based on validation results from previous LIBRA-seq studies. Cells which bound to multiple antigens from different viral families were filtered out to remove polyreactive BCRs, along with any cells from non-HIV donors which bound HIV antigens.

QUANTIFICATION AND STATISTICAL ANALYSIS

Statistical analyses were performed using GraphPad Prism v9.5.0 and v10.1.0. ELISAs were analyzed by fitting a four-parameter logistic regression curve to determine area under the curve (AUC). Neutralization assays were analyzed by fitting a four-parameter logistic curve to interpolate IC₅₀ values. For BLI experiments, binding kinetics were fit using a 1:2 bivalent analyte model or a 1:1 model depending on antibody characteristics. Clustering of CDRH3 sequences was performed using hierarchical clustering based on Levenshtein distances. Model training was monitored via evaluation loss and accuracy using 10% held-out validation data.



Supplemental figures

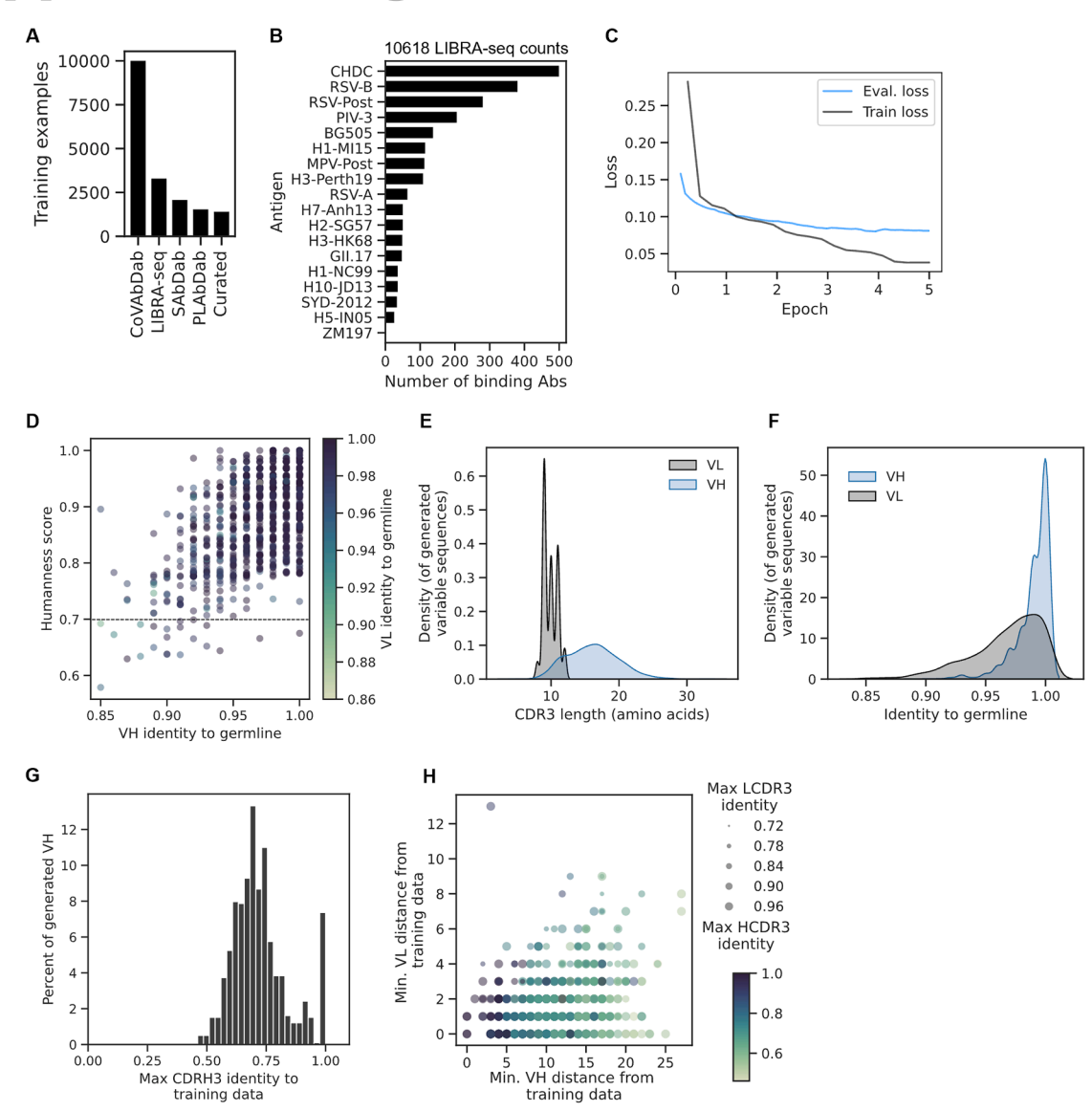


Figure S1. MAGE fine-tuning and generated antibody sequence features, related to Figure 1

- (A) Counts of antibody-antigen pairs in training data grouped by source. A more detailed breakdown is provided in Table S1.
- (B) Counts of binding (LSS > 2 and UMI > 30) cells screened by LIBRA-seq across 4 donors.
- (C) Training and evaluation loss for 5 epochs (iterations over training data) of fine-tuning.
- (D) Scatterplot showing relationship between VH identity and the OASis humanness score for antibodies generated against RBD. Dotted line at humanness score of 0.7 represents the threshold used in antibody selection.
- (E) Distributions of CDR3 length for heavy and light variable sequences in generated antibodies.
- (F) Distributions of percent identity to germ line for variable heavy (VH) and light (VL) chains in antibodies generated against RBD.
- (G) Distribution of the maximum CDRH3 identity between each generated antibody and the training data.
- (H) Distance to the closest training example for the generated VH and VL sequences is shown. Size of the points represents the maximum LCDR3 to any training sequence, and color represents the maximum HCDR3 to any training sequence.



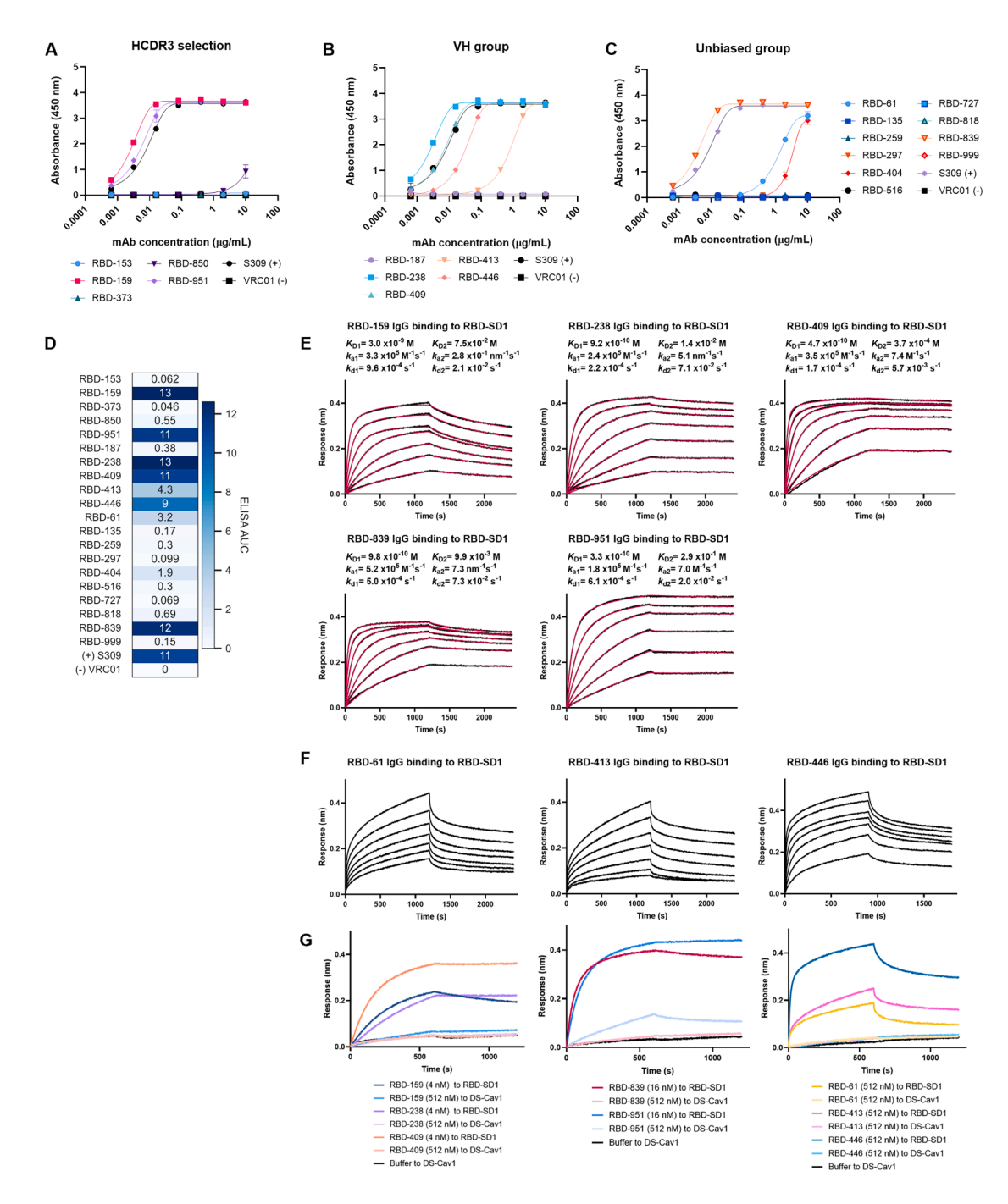


Figure S2. Validation of RBD binding by MAGE-generated antibodies, related to Figure 2

(A–C) ELISA dilution curves for (A) HCDR3 identity selection group, (B) VH identity selection group, and (C) unbiased-selection group. Positive control SARS-CoV-2 RBD-binding antibody (S309) and negative control HIV-1 specific antibody (VRC01) are shown in black.

- (D) ELISA AUCs from curve fitted to dilution series. Same as Figure 2C but includes exact AUC values.
- (E) BLI sensorgrams (also shown in Figure 2E) for the association and dissociation kinetics of high-affinity antibodies binding to immobilized SARS-CoV-2 RBD-SD1. Data (black) were fitted to a 1:2 bivalent analyte model. Curve fits are shown in red. The bivalent analyte model determines kinetic parameters for the first binding event (KD1, ka1, and kd1), representing affinity of binding and for avid binding of the second antibody arm (KD2, ka2, and kd2).
- (F) BLI sensorgrams for binding of low-affinity antibodies to immobilized SARS-CoV-2 RBD-SD1. Data were single reference subtracted and are shown in black. (G) BLI sensorgrams showing antibody specificity for SARS-CoV-2 RBD. Binding was measured for antibodies to immobilized SARS-CoV-2 RBD-SD1 or prefusion-stabilized RSV F (DS-Cav1).



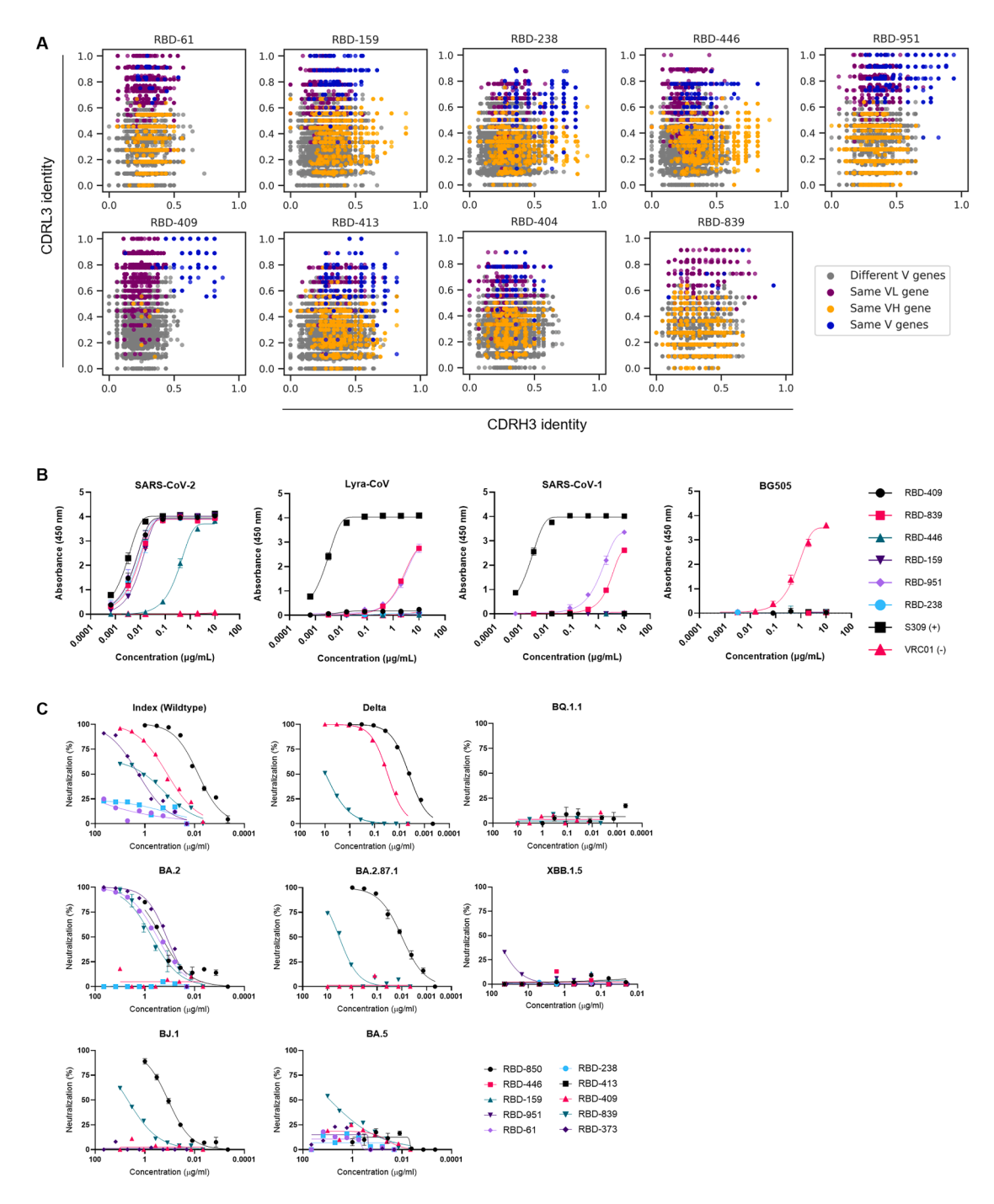


Figure S3. Sequence characteristics and functional properties of RBD-binding antibodies, related to Figure 3

(A) Similarity of designed RBD binders to published RBD-specific antibodies from the CoV-AbDab. Identity is calculated as Levenshtein distance, divided by length of the longer CDR sequence. Pairs are colored based on matching of the V genes.

(B) ELISA dilution curves for RBD binders against panel of SARS-CoV-2 spike variants. Used to calculate AUC values displayed in Figure 3D.

(C) Neutralization dilution curves from pseudovirus neutralization assays for RBD binders generated by MAGE. Used to calculate IC50 values shown in Figure 3E.



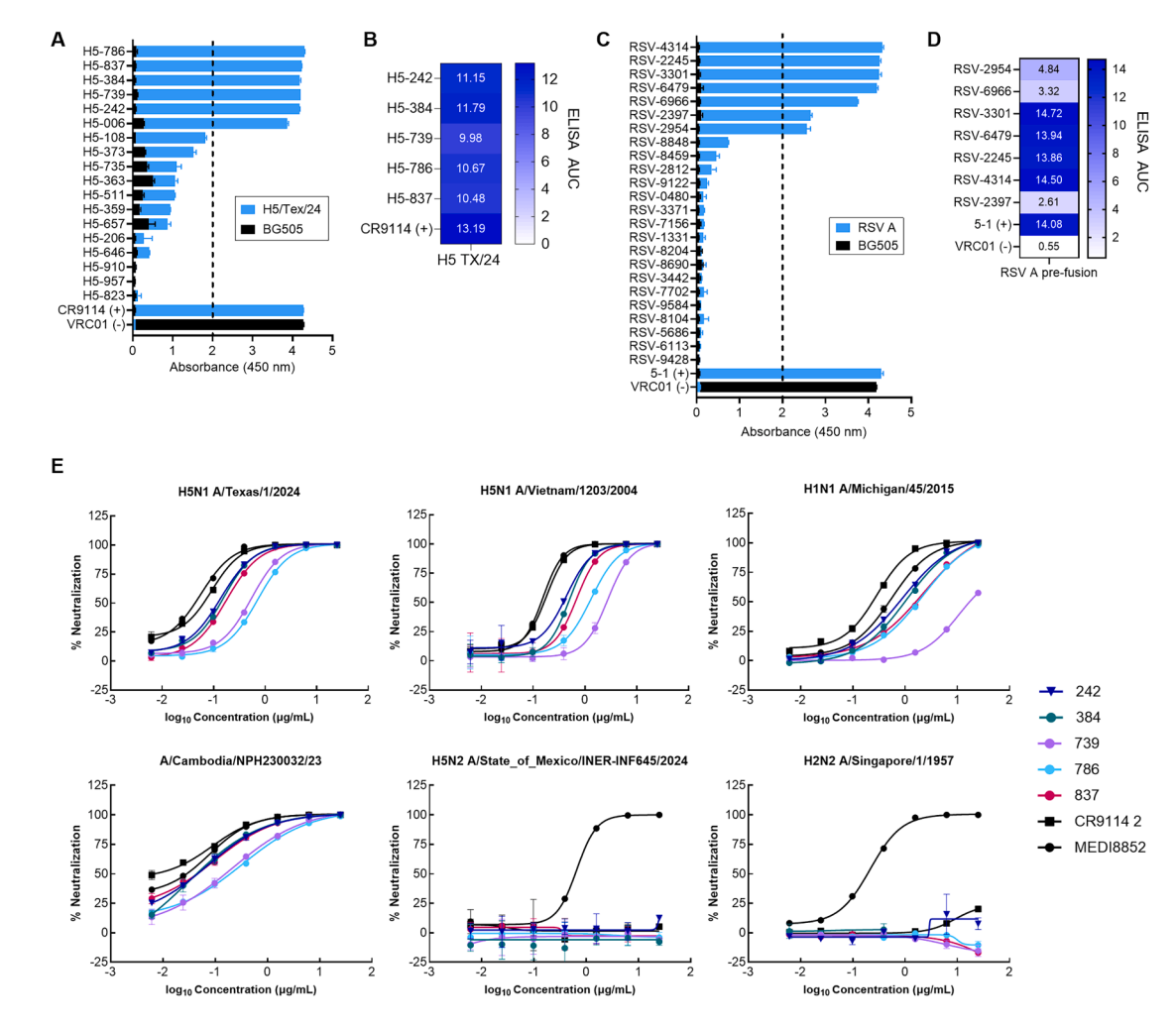


Figure S4. Validation of binding antibodies designed against RSV-A and H5, related to Figures 5 and 6

(A) Initial ELISA screening for MAGE-generated antibodies against H5/TX/24 hemagglutinin was performed at a concentration of 10 µg/mL. Dotted line represents the threshold for further validation.

- (B) ELISA AUC for H5 prefusion binding antibodies. Calculated from curve shown in Figure 5A.
- (C) Initial ELISA screening for MAGE-generated antibodies against RSV-A prefusion was performed at a concentration of 10 μ g/mL. Dotted line represents the threshold for further validation.
- (D) ELISA AUC for RSV-A prefusion binding antibodies. Calculated from curve shown in Figure 6A.
- (E) Neutralization dilution curves against hemagglutinin variants. Used to calculate IC₅₀ values shown in Figure 5F.





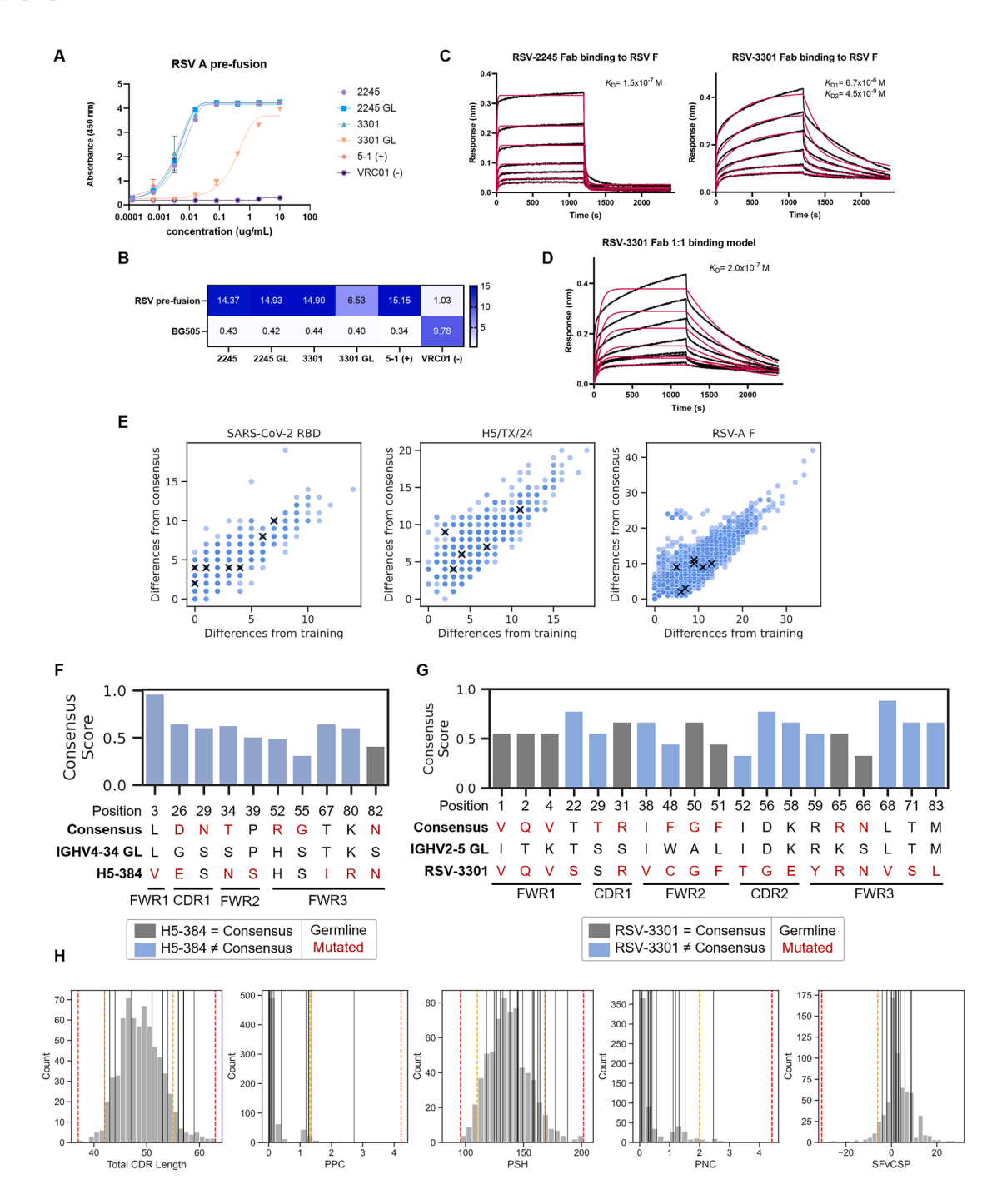


Figure S5. Comparison of MAGE-generated antibodies to germline, training consensus sequences, and therapeutic antibodies, related to Figure 6

(A) ELISA dilution curves for germline-reverted RSV-2245 and RSV-3301 against RSV-A prefusion F. The generated variable sequences were aligned to human germlines, then VH sequences up to CDRH3 were replaced with germline residues.

(B) AUC values for germline-reverted ELISA dilution curves.

(C) BLI sensorgrams for binding of RSV-2245 and RSV-3301 Fabs to immobilized RSV-A F. Data (black) for RSV-2245 binding were fitted to a 1:1 binding model to determine binding affinity (K_D). For RSV-2254, the resulting binding curves displayed rapid saturation during the association phase, followed by a similarly rapid dissociation. A binding affinity (K_D) of 150 nM was determined by fitting the curves to a 1:1 binding model. RSV-3301 binding resulted in curves demonstrating a fast initial association rate that slowed but did not reach saturation during the 1,200-second association step. These curves fit poorly to a 1:1 binding model. Because the RSV-3301 epitope is largely conserved in postfusion (F), simultaneous binding of Fab to pre- and postfusion trimers might be observed. These considerations led us to fit the curves to a heterogeneous ligand model, resulting in apparent K_D values (K_D 1 and K_D 2) of 6.7 μ M and 4.5 nM, respectively. (D) The poorly fitted 1:1 binding model and respective K_D for RSV-3301.





(E) Prompt-specific training antibodies were grouped by VH gene and then aligned using IMGT numbering. From this alignment, the most frequently used residue at each position was used to construct a consensus sequence for each VH gene within the training sequences for each antigen-specificity. Each MAGE antibody was compared to the consensus sequence for that VH gene and the closest training match using Levenshtein distance, for all generated antibodies against SARS-CoV-2 RBD, H5/TX/24, and RSV-A F.

⁽F) H5-384 aligned to the consensus and germline sequences for H5-specific IGHV4-34 antibodies from training. The bar plot represents the consensus score, showing the proportion of training antibodies which use the most common residue at each position, colored based on whether H5-384 contains the consensus residue (gray = consensus, blue = different). Non-germline residues are shown in red.

⁽G) MAGE antibody RSV-3301 aligned to the consensus and germline sequences for RSV-specific IGHV2-5 antibodies from training.

⁽H) TAP scores for validated MAGE antibodies. Gray histogram represents distribution of therapeutic antibodies, with orange lines representing Amber Flag regions and red lines representing Red Flag regions based on suggested risk thresholds1. Black lines represent validated MAGE antibodies across all prompt groups with scores for: total CDR length, patches of positive charge, patches of surace hydrophobicity, patches of negative charge, and structural Fv charge symmetry parameters.





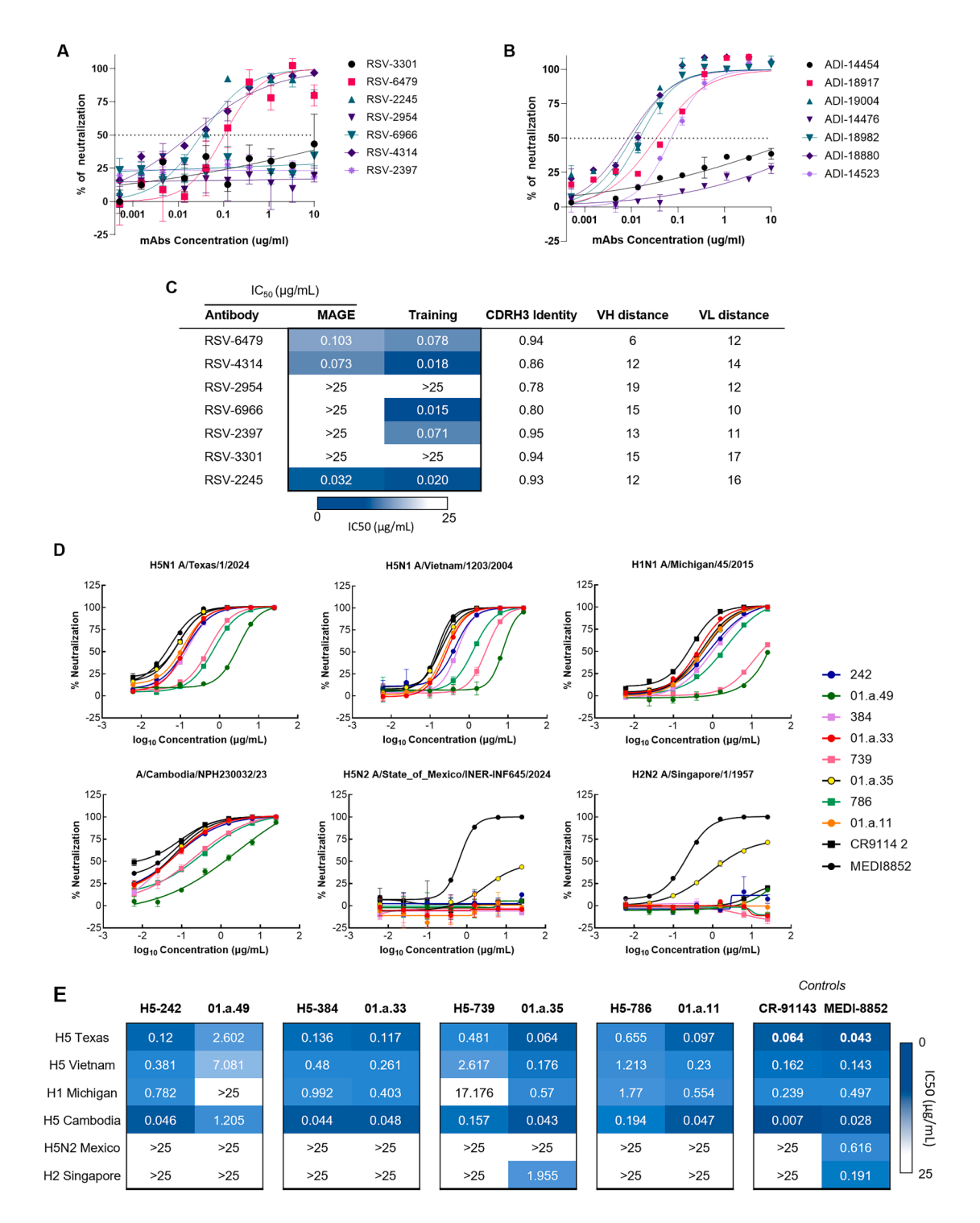


Figure S6. Comparison of neutralization profiles for MAGE antibodies and closest training matches, related to Figures 5 and 6

(A and B) Neutralization dilution curves for (A) MAGE-generated RSV antibodies and (B) their closest training matches.

(C) Summary of IC₅₀ values for antibodies from (A and B), along with sequence feature comparisons based on Levenshtein distance and identity (distance normalized by sequence length).

(D) Neutralization dilution curves for MAGE-generated H5 antibodies and their closest training matches against hemagglutinin subtypes.

(E) IC_{50} values from (D), grouped by MAGE antibody and closest training match.



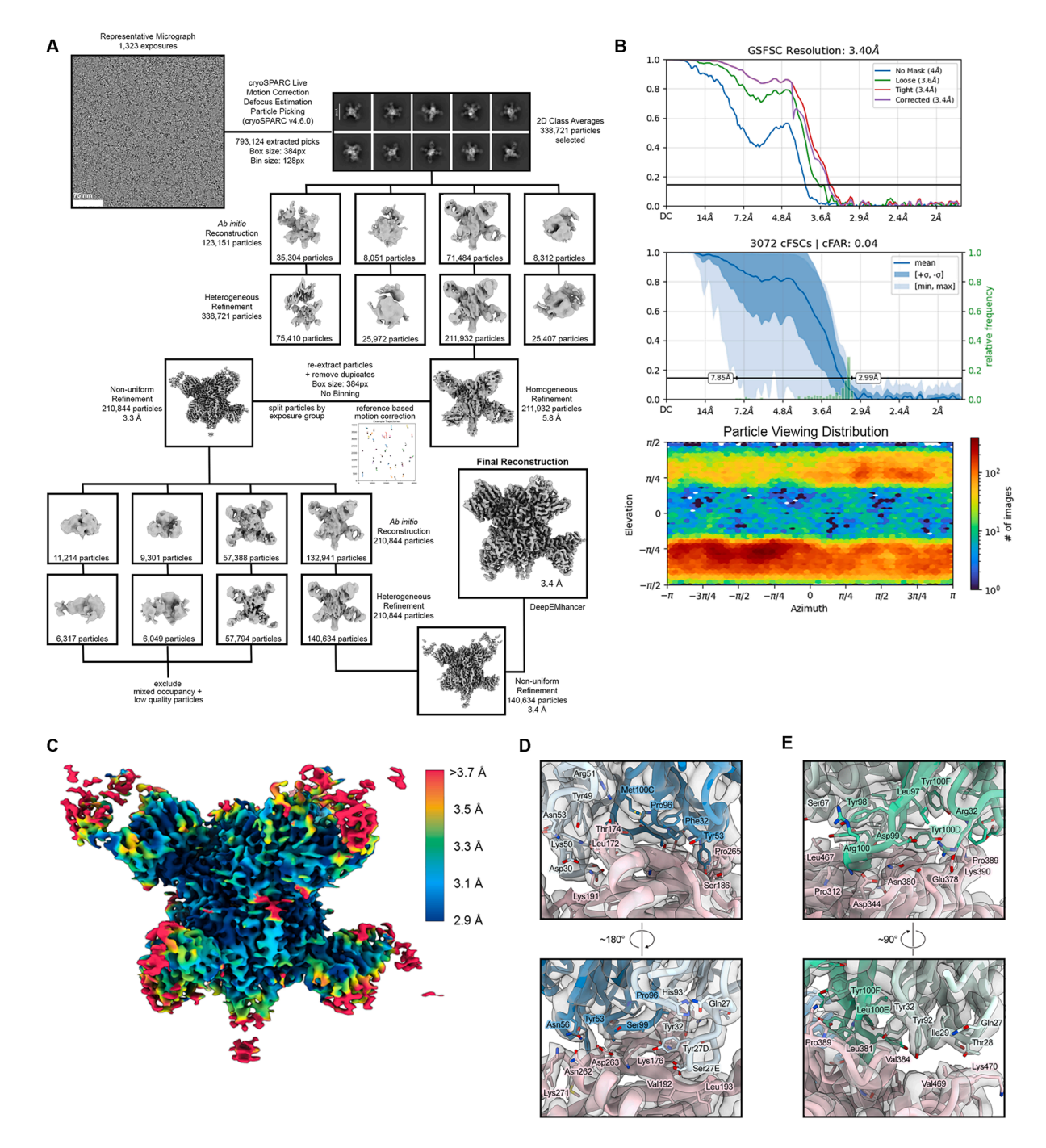


Figure S7. Cryo-EM experimental details for RSV-A F complex with RSV-3301 and RSV-2245, related to Figure 7

- (A) Cryo-EM data processing workflow.
- (B) Gold-standard Fourier shell correlation, conical Fourier shell correlation, and viewing distribution plots for the RSV F + Fab RSV-2245 + Fab RSV-3301 refinement.
- (C) The final map for the RSV F + Fab RSV-2245 + Fab RSV-3301 complex, colored according to local resolution.
- (D) The binding interface for RSV-2245 and RSV-A F. The model is shown with RSV-A F colored pink, the 2,245 heavy chain colored blue, and the 2,245 light chain colored light blue. The map is partially transparent gray.
- (E) The binding interface for RSV-3301 and RSV-A F. The 3,301 heavy chain is colored green, and the 3,301 light chain is colored light green.